Regd. No. C-3911

VOL. 35 **INDIAN JOURNAL OF PHYSICS** No. 1

(Published in collaboration with the Indian Physical Society)

AND

VOL. 44 **PROCEEDINGS** No. 1

OF THE

INDIAN ASSOCIATION FOR THE CULTIVATION OF SCIENCE

JANUARY 1961

PUBLISHED BY THE
INDIAN ASSOCIATION FOR THE CULTIVATION OF SCIENCE
JADAVPUR, CALCUTTA 32

Annual Subscription—
Inland Rs. 25.00
Foreign £ 2-10-0 or $ 7.00

NOTICE
TO INTENDING AUTHORS

1. Manuscripts for publication should be sent to the Assistant Editor, Indian Journal of Physics, Jadavpur, Calcutta-32.

2. The manuscripts submitted must be type-written with double space on thick foolscap paper with sufficient margin on the left and at the top. The original copy, and not the carbon copy, should be submitted. Each paper must contain an ABSTRACT at the beginning.

3. All REFERENCES should be given in the text by quoting the surname of the author, followed by year of publication, *e.g.*, (Roy, 1958). The full REFERENCE should be given in a list at the end, arranged alphabatically, as follows; MAZUMDER, M. 1959, *Ind. J. Phys.*, **33**, 346.

4. Line diagrams should be drawn on white Bristol board or tracing paper with black Indian ink, and letters and numbers inside the diagrams should be written neatly in capital type with Indian ink. The size of the diagrams submitted and the lettering inside should be large enough so that it is legible after reduction to one-third the original size. A simple style of lettering such as gothic, with its uniform line width and no serifs should be used, *e.g.*,

A·B·E·F·G·M·P·T·W·

5. Photographs submitted for publication should be printed on glossy paper with somewhat more contrast than that desired in the reproduction.

6. Captions to all figures should be typed in a separate sheet and attached at the end of the paper.

7. The mathematical expressions should be written carefully by hand. Care should be taken to distinguish between capital and small letters and superscripts and subscripts. Repetition of a complex expression should be avoided by representing it by a symbol. Greek letters and unusual symbols should be identified in the margin. Fractional exponents should be used instead of root signs.

EFFECTS OF COULOMB FRICTION ON THE PERFORMANCE OF A SERVOMECHANISM HAVING BACKLASH. PART II—TRANSIENT RESPONSE CONSIDERATIONS

A. K. MAHALANOBIS

Institute of Radiophysics and Electronics, University College of Technology, Calcutta

(*Received, October* 9, 1960)

ABSTRACT. The paper gives results of analysis of the effects of coulomb friction on the transient response of a servo system containing backlash in the output coupling. First, the qualitative aspects of the transient response characteristics are discussed with the help of frequency response methods; next, a quantiative discussion of the same is provided with the help of a piece-wise linear solution of the characteristic differential equations. Simulator results in support of the theoretical observations are also given.

INTRODUCTION

In a previous paper the effects of coulomb friction on the stability of sustained oscillations in a second order servomechanism having backlash in the output coupling was discussed (Mahalanabis, 1960). The coulomb friction has been taken to be present in the driving member. A describing function was developed for the motor under the action of the nonlinear friction; it was discussed how presence of coulomb friction helps to avoid sustained oscillations that are otherwise produced by the system backlash.

Beside the question of the stability of sustained oscillations the stability of the response of a system in the transient state is also of considerable interest to servo designers. In the present paper the relative stability of a servo system affected by the two nonlinearities under consideration viz. backlash and coulomb friction has been analysed.

It is to be mentioned that the discussions that follow have been based on the results of application of two methods. First, the results of application of the frequency response method are presented. These are necessarily of approximate nature but are nevertheless of interest since this is perhaps the most nearly generalised approach available at present for nonlinear systems analysis. More accurate data on the transient response of the system concerned are provided by solution of the piece-wise linear differential equations that characterise the system.

Finally, the response of a system simulated on an electronic analogue computer for step displacement inputs is presented as an experimental aid to the understanding of the system transient behaviour.

SYSTEM UNDER CONSIDERATION

The system under consideration has been described in part I (Mahalanobis, 1960) in some details and will be only briefly outlined here for the sake of convenience. The system is shown in Fig. 1 in the schematic form. Nonlinearities

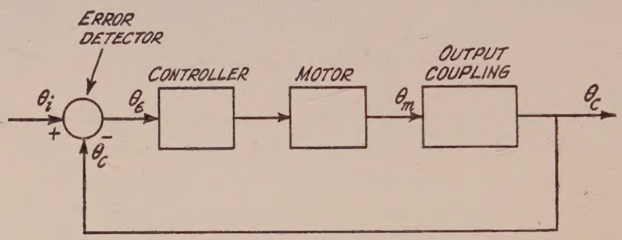

Fig. 1. System under consideration

are assumed in (i) the motor shaft whose motion is taken to be subject to both viscous and coulomb frictions and (ii) the output coupling unit which is taken to have backlash. The load is assumed to be a resistive one so that the nonlinear characteristics resulting from the coupling-unit backlash is as shown in Fig. 2. In Fig. 3 is depicted the composite friction characteristics of the motor.

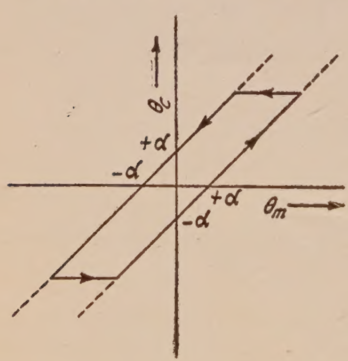

Fig. 2. Coupling unit characteristics.

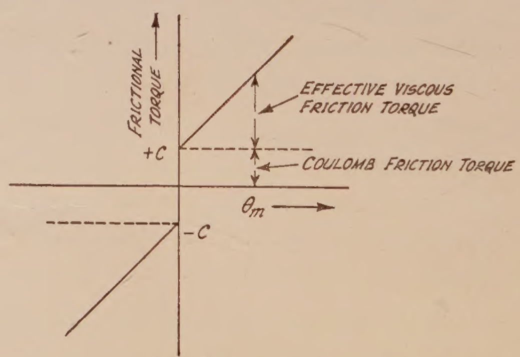

F.ig 3. Motor friction characteristics.

As has been derived in appendix I of part I the dynamics of the system in Fig. 1 is described by the following equations:

$$T_m\ddot{\theta}_m+\dot{\theta}_m+F = k\theta_\varepsilon \qquad \dots \quad (1)$$

$$\theta_\varepsilon = \theta_i-\theta_c \qquad \dots \quad (2)$$

where, θ_m—motor shaft position
θ_i—input shaft position
θ_c—output shaft position
T_m—motor time constant
F—coulomb friction torque,
and K—a constant, being the velocity-constant of the system that results if the nonlinearities in Fig. 1 are neglected.

The backlash characteristics shown in Fig. 2 relates the motor shaft position θ_m and the load shaft position θ_e and can be represented mathematically as

$$\left.\begin{aligned} \theta_c &= \theta_m - \alpha \frac{\dot{\theta}_c}{|\dot{\theta}_c|};\ \dot{\theta}_c \neq 0 \\ |\theta_m - \theta_c| &< \alpha;\ \dot{\theta}_c = 0 \end{aligned}\right\} \quad \dots \quad (3)$$

α being the backlash half width.

And, the coulomb friction torque F is given by

$$\left.\begin{aligned} F &= C \frac{\dot{\theta}_m}{|\dot{\theta}_m|}\ ;\ \dot{\theta}_m \neq 0 \\ -C < F &< C\ ;\ \dot{\theta}_m = 0 \end{aligned}\right\} \quad \dots \quad (4)$$

C being the coulomb friction torque constant.

Eqs. (1) to (4) completely describe the system in Fig. 1.

SYSTEM TRANSIENT RESPONSE FROM FREQENCY RESPONSE DATA

(a) *General*

If the nonlinearities in Fig. 1 are assumed absent the time response of the system has definite correlationships with its frequency response. In presence of the nonlinearities there is of course no basis for such correlationship (the superposition principle being no longer valid). However, in the describing function method the nonlinearity is replaced by a slowly varying quasi-linear transfer function and it is still possible to obtain the transient response from the frequency response data, though such deductions are necessarily of approximate nature (Kochenburger 1950 and 1953). For this purpose the system in Fig. 1 is represented in the block diagram form in Fig. 4. The block $G_c(\theta_m)$ represents the describing function of the coulomb friction device and is given by (Hass 1953)

$$G_c(\theta_m) = \frac{4C}{\pi} \frac{1}{|\dot{\theta}_m|} \quad \dots \quad (5)$$

The block $G_B(\theta_m)$ represents the describing function of the coupling unit having backlash and is given by (Nichols 1953)

$$G_B(\theta_m) = [\beta^2+\gamma^2]^{\frac{1}{2}} \; ; \; \underline{/-\tan^{-1}(\gamma/\beta)} \qquad \text{... (6)}$$

$$\beta = \frac{1}{\pi}\,[\cos^{-1}(2n-1)+2(1-2n)\sqrt{n(1-n)}] \qquad \text{... (7)}$$

and

$$\gamma = \frac{4}{\pi}\, n(1-n) \qquad \text{... (8)}$$

where $n = \alpha/\hat{\theta}_m$, the normalised blacklash width.

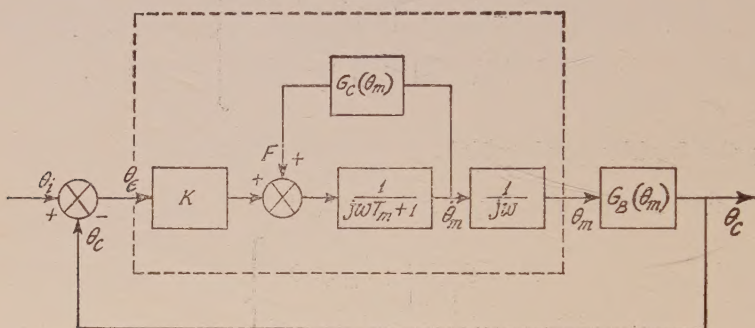

Fig. 4. Frequency response representation of the system.

The frequency response transfer function of the portion in Fig. 4 shown within the dotted box representing the motor with the coulomb friction is easily seen to be given by

$$G(j\omega, \theta_m) = \frac{K}{j\omega(j\omega T_m+1)+j\,\dfrac{4B}{\pi}} \; ; \qquad \text{... (9)}$$

$$B = \frac{C}{\hat{\theta}_m} \qquad \text{... (10)}$$

The total forward-loop transference of the system is then

$$\frac{\theta_C}{\theta_\varepsilon}\,(j\omega,\; \theta_m) = G(j\omega,\, \theta_m)\times G_B(\theta_m) \; ; \qquad \text{... (11)}$$

and the closed-loop transference is accordingly,

$$\frac{\theta_C}{\theta_i}\,(j\omega, \theta_m) = \frac{G_B(\theta_m)}{G(j\omega, \theta_m)^{-1}+G_B(\theta_m)} \qquad \text{... (12)}$$

The right-hand side of Eq. (12) incorporates the effects of the nonlinearities on the system frequency response. This is clearly dependent on both amplitude and frequency of the input signal. It is most convenient to assume the input signal to be a periodic function of time such that $\theta_m(t)$ varies sinusoidally i.e. $\theta_m(t) = \hat{\theta}_m \sin \omega t$. Then, using Eqs. (6) to (10) and Eq. (12) the closed-loop transfer function can be computed as a function of the frequency for a number of assumed values of the amplitude $\hat{\theta}_m$. These computations are conveniently carried out graphically in the manner outlined below:

The describing function $-G_B(\theta_m)$. is plotted in the complex plane as an amplitude locus. On the same plane are superposed plots of the frequency loci of $G(j\omega, \theta_m)^{-1}$ each locus being drawn for a specific value of $\hat{\theta_m}$. In Fig. 5 are shown these plots for the system in Fig. 4 for the assumed values of $K = 10$ and $T_m = 1$, using the normalised signal parameters n and B.

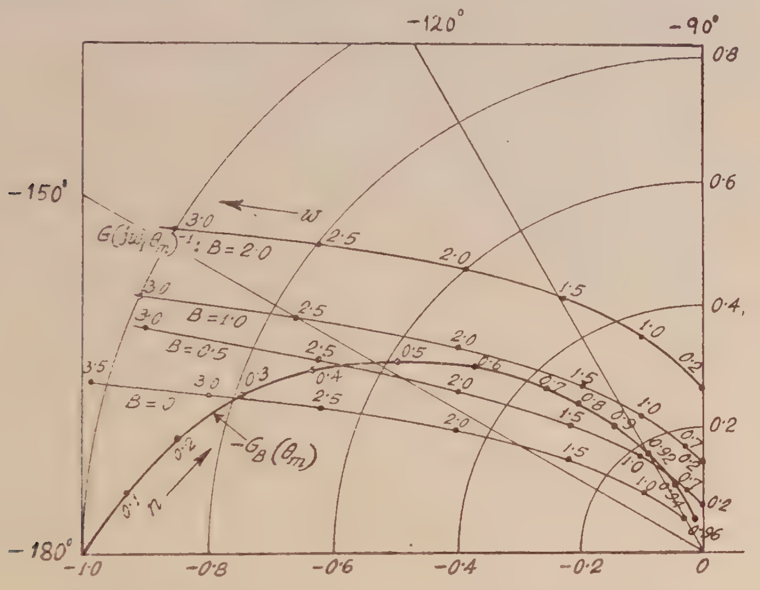

Fig. 5. Plots of $G(j\omega, \theta_m)^{-1}$ and $-G_B(\theta_m)$in the complex plain.

Let us assume that the frequency response of the system corresponding to a signal amplitude $\hat{\theta}_m = \hat{\theta}_{m1}$ is desired. This is easily done by locating the point $G_B(\theta_{m1})$ on the amplitude locus (marked P in Fig. 5) and considering the frequency locus $G(j\omega, \theta_{m1})^{-1}$. Then at any frequency ω_1 (corresponding to the point Q in Fig. 5) the frequency response modulus is given by the ratio

$$\left| \frac{\theta_C}{\theta_i} \right|_{\substack{\hat{\theta}_m = \hat{\theta}_{m1} \\ \omega = \omega_1}} = \left| \frac{OP}{PQ} \right| \qquad \text{... (13)}$$

This ratio, if evaluated for a number of frequencies over the range of interest gives, when plotted against the frequency, the system frequency response corresponding to the signal amplitude $\hat{\theta}_m = \hat{\theta}_{m1}$. If this whole procedure is repeated for a number of values of $\hat{\theta}_m$ the frequency response of the system is evaluated as a function of amplitude and frequency. This can be done for different amounts of coulomb friction.

In Figs. 6(a), (b) and (c) are shown the frequency response curves of the system in Fig. 4 as obtained from the loci of Fig. 5 for three different cases corresponding

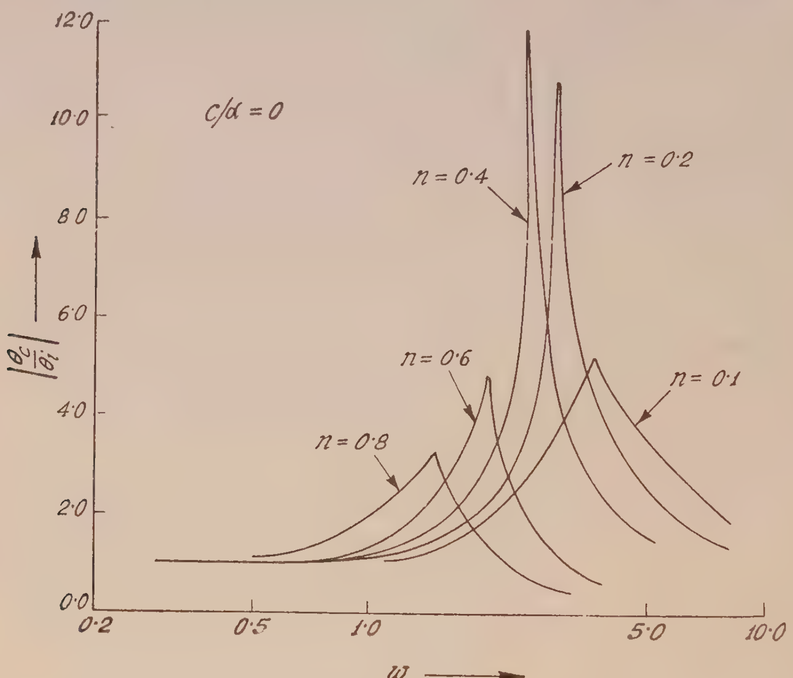

Fig. 6. (a) Frequency response plots : C/α=0

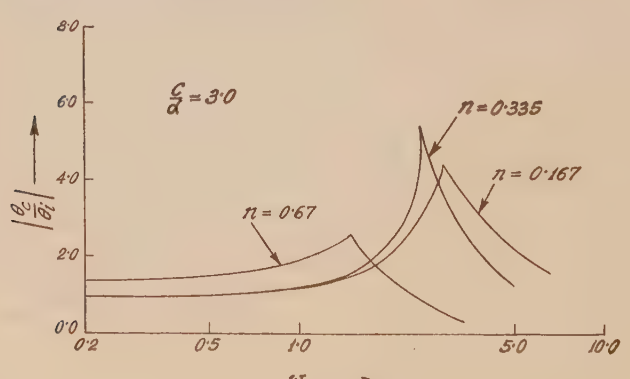

Fig. 6(b) C/α=3.0

to $C/\alpha = 0$, 3.0 and 5.0. The peak value of the ratio $|\theta_C/\theta_i|$ gives a measure of the system's relative stability and the frequency ω_r at which this peak occurs gives a measure of the system's speed of response.

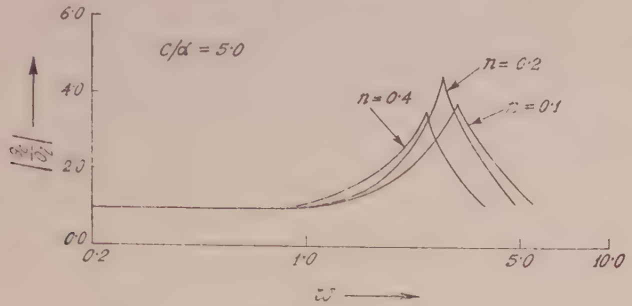

Fig. 6(c) $C/\alpha = 5.0$

(b) *Effects of the nonlinearities*

The effects of the two nonlinearities viz. backlash and coulomb friction, on the degree of stability as well as the speed of the response of the system can be seen from the frequency response curves of Fig. 6. In order to bring out the effects of the coulomb friction we proceed as follows :

Let us first assume that the motor is characterised by a truly linear friction characteristics so that instead of the quasilinear describing function $G(j\omega, \theta_m)$ given by Eq. (9) the motor is characterised by linear transfer function

$$G(j\omega) = \frac{K}{j\omega(j\omega T_m+1)} \qquad \ldots \quad (14)$$

The resultant frequency response curves are shown in Fig. 6(a). These curves incorporate the effects of backlash alone. The values of $|\theta_C/\theta_i|$ (θ_m) and $\omega_r(\theta_m)$ obtained from these curves are plotted against the normalised amplitude n in Figs. 7(a) and (b) respectively (curves marked $C/\alpha = 0$). It is seen that the magnitude of the ratio $|\theta_c/\theta_i|$ increases with falling signal amplitude (i.e. with n increasing) until it reches an infinitely large value (at a signal amplitude corresponding to $n = .3$ in Fig. 8). This indicates a possibility of sustained oscillation (of this amplitude) in the system. The reduction of the magnitude of the response amplitude at still smaller values of the signal amplitude is of course to be expected since the effective gain approaches zero due to the backlash dead-zone. The region of instability (round about the signal amplitude of about 3.3 in the present case) is of the order of backlash width. It can be concluded therefore that the presence of backlash causes the system stability to be impaired primarily at comparatively small signal levels. Also there is a slight reduction in the values of $\omega_r(\theta_m)$ at smaller signal amplitudes thus reducing the system's speed of response.

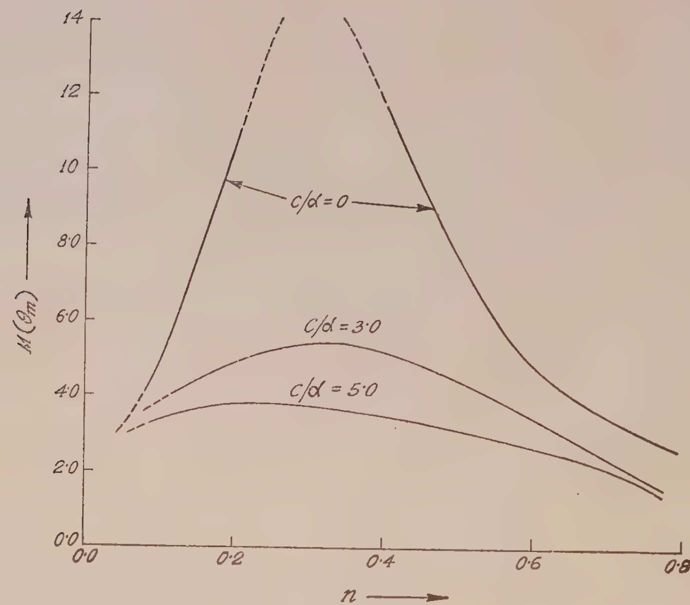

Fig. 7. Plots of (a) frequency-response peak $M(\theta_m)$

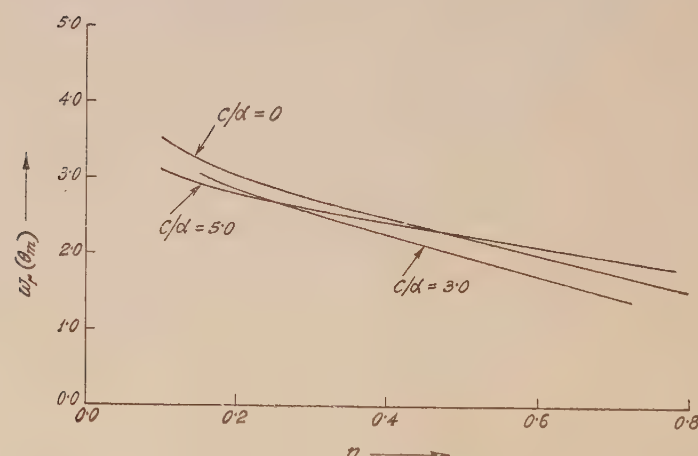

Fig- 7(b). frequency of occurrence of the peak $\omega_r(\theta_m)$ against n.

If now the same parameters $|\theta_e/\theta_i|(\theta_m)$ and $\omega_r(\theta_m)$ are evaluated from the response curves of Figs. 6(b) and (c) the results of addition of the coulomb friction becomes evident. These also are plotted in Fig. 7 against n (curves marked $C/\alpha = 3.0$ and $C/\alpha = 5.0$) in order to emphasize the effects of the coulomb friction. It is seen that for the conditions specified the value of the frequency response peak as also the frequency show much less dependence on the signal amplitude; not only are the sustained oscillations avoided but addition of adequate coulomb friction can effectively improve the system's damping at small signal levels.

These results are in fact to be expected from the form of the describing function $G(j\omega, \theta_m)$ as given by Eq. (9). It is seen that the effect of considering only the fundamental component of the coulomb friction torque for an assumed sinusoidal motor speed is to replace the nonlinear friction by an equivalent amplitude-dependent viscous friction $4C/\pi|\dot{\theta}_m|$, a quantity which is predominant at comparatively smaller values of $\hat{\theta}_m$.

TIME RESPONSE FROM THE SOLUTION OF THE CHARACTERISTIC EQUATIONS

The discussions in the previous sections give a qualitative picture of the effects of coulomb friction on the stability and the speed of the response of a servo system having backlash in the output coupling. A more quantitative analysis of the problem is, however, possible by following a method suggested by Oldenburg and Sartorius (1948). This consists of solving certain piecewise linear differential equations which characterise the system under the stipulated conditions. To set up these equations we start with a typical step response of a system which has low damping. This is indicated in Fig. 8; a response which exhibits some oscillations before attaining the steady state value. Taking $t = 0$ at the instant at which

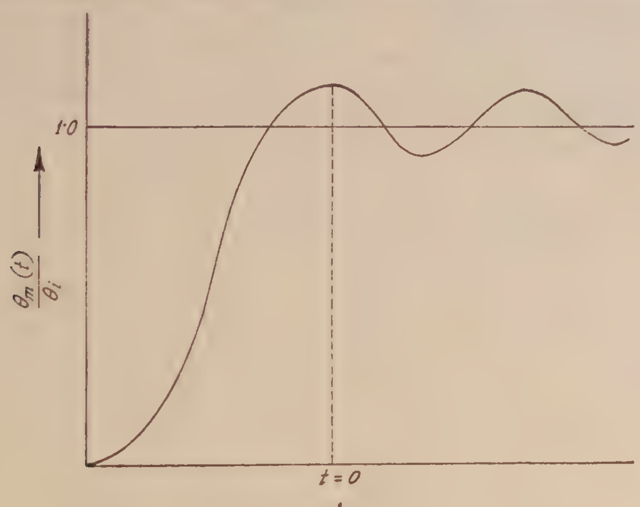

Fig. 8. A typical step input response of the system.

the first overshoot occurs the function $\theta_m(t)$ in Fig. 8 can be considered as a damped sinusoid, at least during the first few oscillations. The relationship between the motor shaft and outputshaft positions can then be set up as

$$\left.\begin{aligned} \theta_c &= \hat{\theta}_{m0} - \alpha; \quad 0 \leqslant \omega t \leqslant \theta_2 \\ &= \theta_m + \alpha; \quad \theta_2 \leqslant \omega t \leqslant \pi \end{aligned}\right\} \quad \ldots \quad (15)$$

$$\left.\begin{array}{ll}\text{where } \hat{\theta}_{m0} = \text{the initial amplitude of oscillation} & \\ \text{and} \quad \theta_2 = \cos^{-1}(1-2\alpha/\hat{\theta}_{m0}) & \end{array}\right\} \quad \ldots \quad (16)$$

These quantities are defined as in Fig. 9. Now substituting for θ_c in Eq. (1) and setting $\theta_i = 0$ we get the two following equations which are valid for the two sections of the half period of $\theta_m(t)$ defined in Eq. (15). Thus, for

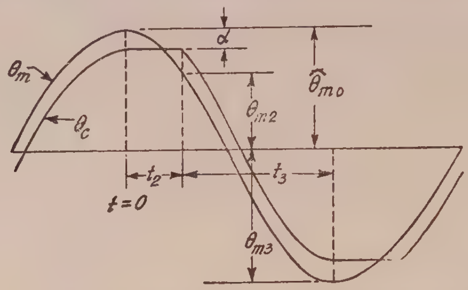

FIG. 9. Waveforms illustrating the boundary conditions.

$$0 \leqslant t \leqslant \theta_2/\omega,$$

$$T_m \frac{d^2\theta_m}{dt^2} + \frac{d\theta_m}{dt} = C - K(\hat{\theta}_{m0} - \alpha) \quad \ldots \quad (17)$$

the boundary conditions being

$$t = 0, \qquad \theta_m = \hat{\theta}_{m0} \quad \text{and} \quad \dot{\theta}_m = 0$$

and $\quad t \Rightarrow t_2(\text{say}) = \theta_2/\omega, \quad \theta_m = \hat{\theta}_{m0} - 2\alpha = \theta_{m2}$ (say)

and $\dot{\theta}_m = [\dot{\theta}_m]_2$ (say), which is a negative quantity.

For the other section using a new independent variable t_1 i.e. for

$$0 \leqslant t_1 \leqslant \theta_3/\omega \text{ (say)},$$

$$T_m \frac{d^2\theta_m}{dt_1^{\,2}} + \frac{d\theta_m}{dt_1} + K\theta_m = C - K\alpha \quad \ldots \quad (18)$$

—the boundary conditions being

$t_1 = 0, \quad \theta_m = \theta_{m2} \quad$ and $\quad \dot{\theta}_m = [\dot{\theta}_m]_2$, as obtained from the previous section,

and $\qquad t_1 = t_3 = \theta_3/\omega, \qquad \theta_m = \theta_{m3}$(say) and $\dot{\theta}_m = 0$.

Eqs. (17) and (18), subject to the specified boundary conditions, can now be solved to give the nature of the system response during the half period in question. The solution can then be used to compute such transient response parameters as the half period decrement and the half period of the transient oscillations. The results of these computations involve the nonlinearities and bring out their effects on the system response. In terms of the symbols used above these two parameters require evaluation of θ_{m3} and (t_2+t_3). The procedure for the purpose is outlined below :

Solution of Eq. (17) gives

$$\theta_m(t) = \hat{\theta}_{m0} - k(t - T_m + T_m e^{-t/T_m}) \quad \dots \quad (19)$$

where

$$k = K(\hat{\theta}_{m0} - \alpha) - C \quad \dots \quad (20)$$

Substituting $t = t_2 = \theta_2/\omega$,

$$\theta_{m2} = \hat{\theta}_{m0} - 2\alpha = \hat{\theta}_{m0} - k(t_2 - T_m D) \quad \dots \quad (21)$$

where

$$D = 1 - e^{-t_2/T_m} \quad \dots \quad (22)$$

Eqs. (21) and (22), when solved, gives t_2.

Solution of Eq. (18) gives

$$\theta_m(t_1) = \frac{C}{K} - \alpha + \left(\alpha - \frac{C}{K} + \theta_{m2}\right) e^{-\rho t_1} \cos \lambda t_1$$

$$+ \frac{1}{\lambda}\left[\rho\left(\alpha - \frac{C}{K} + \theta_{m2}\right)\right] e^{-\rho t_1} \sin \lambda t_1 \quad \dots \quad (23)$$

where ρ and λ are two parameters given by

$$\rho = \frac{1}{2T_m} \; ; \quad \rho^2 + \lambda^2 = K/T_m \quad \dots \quad (24)$$

Substitution of the terminating condition in (23) leads to

$$\tan \lambda t_3 = \frac{\lambda D/\rho}{D-2} \quad \dots \quad (25)$$

This gives t_3.

Also putting $t_1 = t_3$ in (23) we get

$$\theta_{m3} = \frac{C}{K} - \alpha + \frac{\left(\hat{\theta}_{m0} - \alpha - \frac{C}{K}\right)(1 - D + D^2 K T_m)}{1 - D/2} e^{-\rho t_3} \cos \lambda t_3 \quad \dots \quad (26)$$

From (26) we have

$$\frac{\theta_{m3}+\alpha}{\hat{\theta}_{m0}-\alpha}=\frac{C}{K(\hat{\theta}_{m0}-\alpha)}+\frac{\hat{\theta}_{m0}-\alpha-\dfrac{C}{K}}{\hat{\theta}_{m0}-\alpha}\cdot\frac{1-D+D^2KT_m}{1-D/2}\,e^{-\rho t_3}\cos\lambda t_3 \quad \ldots \quad (27)$$

Noting (Fig. 9) that θ_{m3} has a negative value, Eq. (27) can be rewritten as

$$\Delta=\frac{|\theta_{m3}|-\alpha}{\hat{\theta}_{m0}-\alpha}=\frac{\theta_{m0}-\alpha-\dfrac{C}{K}}{\hat{\theta}_{m0}-\alpha}\;\frac{1-D+D^2KT_m}{D/2-1}\,e^{-\rho t_3}\cos\lambda t_3$$

$$-\frac{C}{K(\hat{\theta}_{m0}-\alpha)}$$

$$=\left[1-\frac{C/\alpha}{K(\phi_{m0}-1)}\right]H-\frac{C/\alpha}{K(\phi_{m0}-1)} \quad \ldots \quad (28)$$

where $\phi_{m0}=\hat{\theta}_{m0}/\alpha$—the normalised amplitude.

The left hand side of this equation is easily identified as the half period decrement of $\theta_C(t)$, the load motion. On the right hand side of (28) the factor H represents the half-period decrement of the load motion when the coulomb friction constant C is zero. This factor has been worked out by Nichols (1953) who studied the effects of backlash in a servo system. The effect of the coulomb friction is obviously to reduce this value thus indicating a stabilising action.

For given values of the system constants the half period decrement given by (28) and the half period given by $T/2=t_2+t_3$ as obtained from Eqs. (21) and (22) and Eq. (25) respectively, can be computed. The results are plotted in Fig. 10 against the normalised signal amplitude $\phi_{m0}-1=(\hat{\theta}_{m0}-\alpha)/\alpha$ using the normalised coulomb friction constant C/α as a parameter. The curves of Fig. 10 point out that the effects of the coulomb friction predominate when the signal amplitude is small. In general an increase in the value of C results in a reduction of Δ and slight increase of the half-period. The results are in agreement with the earlier conclusions of the qualitative discussions.

RESULTS OF SIMULATOR STUDIES

The arrangement of the simulator has been discussed in reference 1 and is shown in Fig. 11. The simulator is capable of varying the normalised coulomb friction constant C/α as well as the gain K. The response $\theta_m(t)$ for step displacement inputs under different conditions of gain and the constant C/α have been

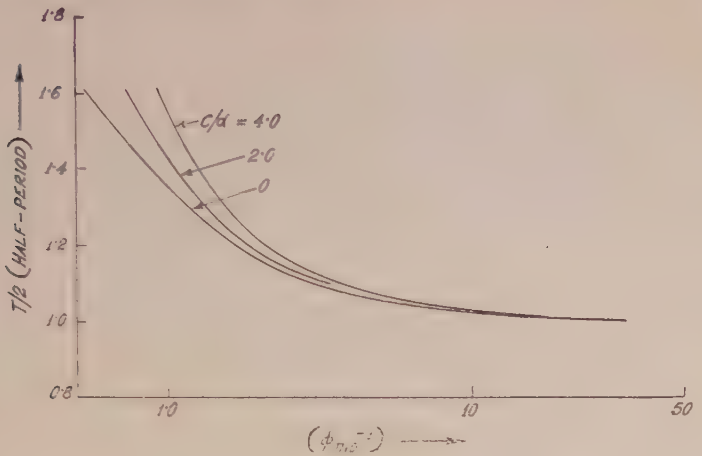

Fig. 10(a). Plots of the half-period decrement Δ against $\phi_{m_s}{}^{-1}$.

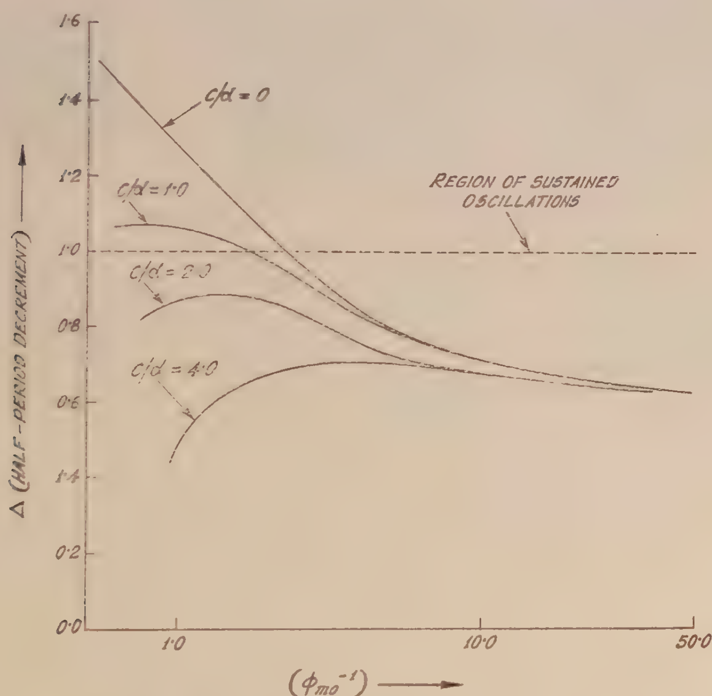

Fig. 10(b). Plots of half period T/2 against $\phi_{m0}{}^{-1}$.

obtained and are displayed in the traces of Figs. 12(a) and (b). In Fig. 12(a) are shown traces of response for a gain $K = 4.0$ and $C/\alpha = 0$, 2.5 and 4.0. In Fig. 12(b) are shown traces of the response for $K = 2.0$ and $C/\alpha = 0$, 2.5 and 4.0. The stabilising actions of the columb friction are clearly displayed by these traces.

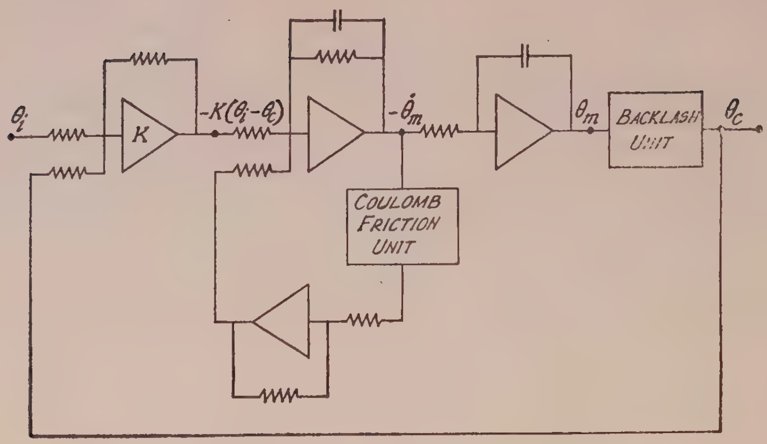

Fig. 11. Simulator set up for the system.

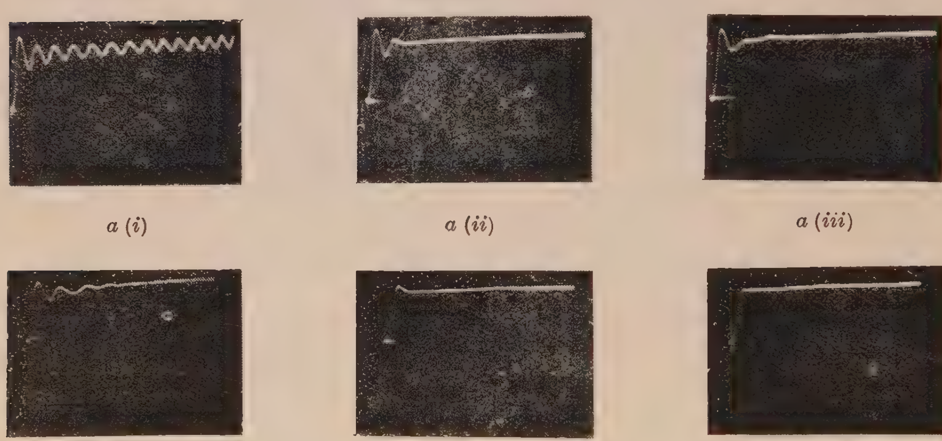

a (*i*) *a* (*ii*) *a* (*iii*)

b (*i*) *b* (*ii*) *b* (*iii*)

Fig. 12. Traces of step responses obtained with the help of the simulator:
(a) $K=4.0$; $C/\alpha=0$, 2.5 and 4.0
(b) $K=2.0$; $C/\alpha=0$, 2.5 and 4.0

CONCLUSIONS

The frequency response data indicate that the presence of coulomb friction in a servomechanism results in an increase of the effective system damping at relatively low signal amplitudes. If the servo system has backlash in the output coupling, coulomb friction can accordingly provide a proper compensation for the backlash effects. Solutions of the piece-wise linear differential equations which characterise the system having the two nonlinearities can be obtained to provide with quantitative data regarding the effects of the two nonlinearities on such transient response parameters as the half period decrement and the half period.

Conclusions drawn from these computations are corroborated by the results of analogue computer studies.

ACKNOWLEDGMENT

The author is greatful to Prof. J. N. Bhar for his guidance and to Dr. A. K. Choudhury for discussions. The award of a scholarship by the Government of India is also thankfully acknowledged.

REFERENCES

Haas, V. B., 1953, *Trans. A. I. E. E.*, **72**, Part 2, pp. 119-123.

Kochenburger, R. J., 1950, *Trans. A.I.E.E.*, **69**, Part 1, 270.

Kochenburger, R. J., 1953, *Trans. A.I.E.E.* **72**, Part 2, 180.

Mahalanobis, A. K., 1960, A.I.E.E. paper No. DP 60-667.

Nichols, N. B., 1953, *Trans. A.I.E.E.*, **72**, Part 2, 462.

Oldenbourg, R. C. and Sartorius, H., 1948, Dynamics of Automatic Controls (book), Transaction by A.S.M.E., New York, N.Y., pp. 168-173.

RAMAN SPECTRA OF PARA FLUOROTOLUENE AND PHENYL ACETONITRILE IN THE SOLID STATE AT −180°C*

KRISHNA KUMAR DEB

Optics Department, Indian Association for the Cultivation of Science, Calcutta-32

(*Received, December* 12, 1960)

PLATE I

ABSTRACT. The Raman spectra of para fluorotoluene and phenyl acetonitrile have been studied in the liquid state and in the solid state at −180°C and the results have been compared with those reported by previous workers for a few compounds having similar molecules. In the case of para fluorotoluene a strong and broad new Raman line of Raman shift 103 cm^{-1} has been observed. The lines 152 cm^{-1} and 333 cm^{-1} are found to shift considerably with the solidification of the liquid.

In the case of phenyl acetonitrile the Raman line 361 cm^{-1} due to $C\equiv N$ deformation oscillation is found to become very weak but the line 2250 cm^{-1} due to $C\equiv N$ stretching oscillation remains almost unchanged when the liquid is solidified. Further, this compound in the solid state also produces only one new Raman line at 95 cm^{-1}. A strong and broad luminescence band at about 21198 cm^{-1} has also been observed in the spectrum due to the crystals in the solid state at −180°C. The significance of these changes has been discussed.

INTRODUCTION

Raman spectra of some substituted toluenes (Biswas, 1954; Sanyal, 1953) and a few nitriles (Bishui, 1948) in different states were studied in this laboratory and some interesting changes were observed in the spectra with solidification of the substances. In continuation of these investigations the Raman spectra of para fluorotoluene and phenyl acetonitrile in the liquid state and in the solid state at −180°C have been investigated and the results have been discussed in the light of the assignment of the lines made by previous workers.

EXPERIMENTAL

The chemicals used in the present investigation were of chemically pure quality. Para fluorotoluene was supplied by Eastman Kodak Co., U.S.A. and phenyl acetonitrile by Fischer Scientific Co., New York. The liquids were subjected to distillation under reduced pressure before each exposure. The spectro-

* Communicatad by Prof. S. C. Sirkar.

Indian Journal of Physics, Vol. 35, No. 1.

PLATE I

ig. 1. (a) (b)

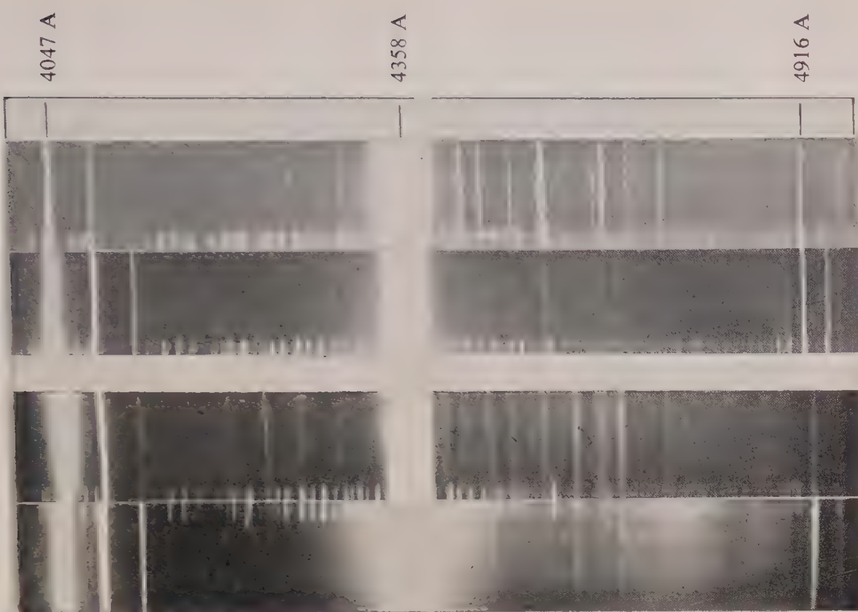

ig. 2. (a) (b)

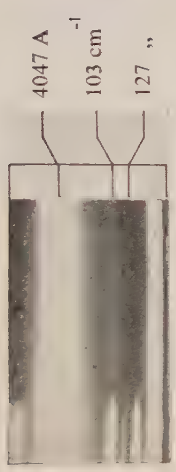

(a)

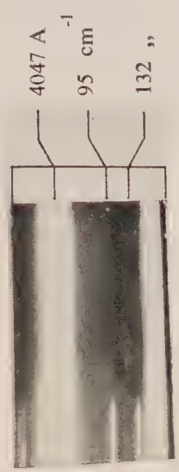

(b)

Fig. 3.

Fig. 1. *(a)* Raman spectra of para fluorotoluene liquid with filter at 28°C
(b) ,, ,, ,, ,, ,, solid at −180°C
Fig. 2. *(a)* Raman spectra of phenyl acetonitrile liquid at 28°C
(b) ,, ,, ,, ,, ,, solid at −180°C
Fig. 3. *(a)* Low frequency Raman lines of para fluorotoluene at −180°C
(b) ,, ,, ,, ,, ,, phenyl acetonitrile at −180°C

grams of the substances in the liquid and solid states and the polarised spectra were recorded with the same arrangements as those used previously (Deb, 1960). The spectra were photographed on Ilford Zenith plates using a Fuess glass spectrograph giving a dispersion of about 11 A per mm in the 4046 A region. The wavelengths were measured with the help of iron arc spectrum recorded on the same plate as a comparison.

RESULTS AND DISCUSSION

The spectrograms are reproduced in Plate I. The observed Raman frequencies together with those reported for the compounds in the liquid state by previous workers are tabulated in Table I and Table II. The polarised and totally depolarised lines are indicated by the letters P and D respectively.

Parafluorotoluene

(a) *Low-frequency lines*

It can be seen from Figs. 1(a) and 1(b) and Table I that in the solid state at $-180°C$, para fluorotoluene yields two new low frequency Raman lines with Raman frequencies 103 cm^{-1} and 127 cm^{-1} respectively. It was previously observed by Sanyal (1953) and Biswas (1954) that para chlorotoluene yields four such lines of Raman frequencies 30 cm^{-1}, 50 cm^{-1}, 85 cm^{-1} and 129 cm^{-1} respectively and para bromotoluene yields only three such lines of Raman frequencies 52 cm^{-1}, 94 cm^{-1} and 133 cm^{-1} respectively. A comparison of these results shows that the frequency about 130 cm^{-1} is present in all these three molecules in the solid state and the other two frequencies 50 and 85 cm^{-1} shown by para chlorotoluene do not change very much when the chlorine atom is replaced by the bromine atom. This shows that the atomic weight of the substituent halogen atoms has very little influence on the frequencies and therefore, they may not belong to any intermolecular vibration in which the adjacent molecules oscillate against each other in the lattice. It also appears that the number of low frequency lines is related very much to the chemical affinity of the molecules. Similar results were observed in the case of halogen substituted benzenes (Mukherjee, 1960). It has been suggested by some previous workers (Sirkar and Bishui, 1946; Sirkar, 1951) that these lines might be due to vibrations in groups of associated molecules in the solid state, but no attempt has been made to indicate the nature of such modes. The analysis of the results obtained with a large number of such compounds is necessary before such modes can be visualised.

(b) *Changes in the position of the other Raman lines with solidification.*

Ferguson *et al.* (1953) have reported the Raman and infrared spectra of para fluorotoluene and have analysed the vibrational bands assuming a point group D_{2h} for the molecule, because the effective mass of the fluorine atom is

nearly the same as that of the CH_3 group taken as a point mass. It can be seen from Table I that the line at 152 cm^{-1} of the liquid, assigned by them to a

TABLE I

Raman spectrum of *p*-fluorotoluene

Liquid: Ferguson *et al.* (1953)	Liquid: Present author	Solid at −180°C: Present author
		103 (8b)
		127 (4)
152	152 (1b)D	
312	310 (1)P	
341	333 (10)D	353 (6)
425		
454	450 (10)P	456 (6)
502	498 (1)D	
638	638 (10)D	638 (6)
695	692 (2)P	
728	722 (2)P	
740		
825	819 (10)P	826 (5)
842	840 (10)P	844 (3)
908	910 (0)	
929		
1003	997 (1)	
1017		
1040		
1061		
1099		
1157	1153 (6)P	1153 (5)
1178		
1214	1214 (10)P	1219 (8)
1221		
1278		
1299	1298 (4) P	1296 (3)
1351		
1382	1380 (6) P	1383 (3)
1404		
1433		
1455	1455 (1b)P	
1495		
1508	1510 (0b)	
1601	1597 (6b)P	1597 (2)
1614		
1858		
1906		
1940		
2385		
2416		
2454		
2740	2736 (2)P	
2871	2876 (4)	
2928	2922 (6) P	2922 (2)
3071	3069 (8)P	3069 (3)

b_{2u} mode of the molecule representing probably an out-of-plane carbon bending vibration shifts to 127 cm^{-1} when the substance is solidified and cooled to $-180°C$. Also the line at 333 cm^{-1} due to a b_{3u} mode shifts under similar conditions to 353 cm^{-1}. In place of two lines at 1601 cm^{-1} and 1614 cm^{-1} observed by the above authors in the case of the liquid, a broad unresolved band at 1597 cm^{-1} is observed in the present investigation. This band, however, becomes sharp when the liquid is frozen. Further, the lines 450 cm^{-1}, 819 cm^{-1} and 840 cm^{-1} of the liquid shift respectively to 456 cm^{-1}, 826 cm^{-1} and 844 cm^{-1} when the liquid is frozen. All these changes suggest some sort of intermolecular association which affects the frequencies of some of the modes of vibration of the single molecule.

Phenyl acetonitrile

(a) *Low-frequency lines*

This compound yields only one low frequency Raman line at 95 cm^{-1} when the liquid is solidified and cooled to $-180°C$. Bishui (1948) studied Raman spectrum of benzonitrile at low temperature and he also observed only one such line at 94 cm^{-1}. A similar compound benzyl chloride, on the other hand, produces four such new lines of Raman shifts 46 cm^{-1}, 62 cm^{-1}, 82 cm^{-1} and 88 cm^{-1} respectively in the solid state at $-180°C$ (Ray, 1951). These results again show that the number of low frequency lines produced by these compounds cannot be satisfactorily explained on the hypothesis of the angular oscillations of the molecules in the crystal lattice, because the number seems to depend on the nature of the individual substituents and not on their masses.

(b) *Changes in the other Raman lines*

In the solid state at $-180°C$, the line 361 cm^{-1} due to $C \equiv N$ deformation oscillation of the molecule in the liquid becomes very weak, but the line 2250 cm^{-1} due to $C \equiv N$ stretching oscillation remains almost unchanged. These changes are similar to those observed in the case of benzonitrile by Bishui (1948) who suggested that $C \equiv N$ deformation oscillation might be restricted in the solid state due to association of the molecules. The results of the present investigation thus confirm this view . The lines 3059 cm^{-1} and 3065 cm^{-1} in the liquid state reported in Tables by Landolt-Börnstein (1951) are not resolved in the spectrograms obtained in the present case, but they appear as a broad band with its centre at 3065 cm^{-1}. With the solidification of the liquid, the band remains broad. Besides these changes mentioned above, frequencies of some other Raman lines of the single molecules are also affected slightly. All these changes again appear to point to the formation of associated groups of molecules in the frozen state of the nitrile compound at the low temperature.

(c) *Luminescence spectra*

In the Raman spectrum of phenyl acetonitrile in the solid state at —180°C a strong and broad luminescence band with its centre at 21198 cm^{-1} has been observed. It is well known now that some substituted benzenes at low temperatures produce such bands in the visible region (Kasha, 1952; Sirkar and Biswas,

TABLE I

Raman spectrum of phenyl acetonitrile

Liquid		Solid at —180°C
Landolt-Bornstein (1951)	Present author	Present author
		95 (6b)
126 (6)	132 (8b)D	132 (4)
216 (2sb)		
235 (3b)	238 (4b)D	243 (3)
322 (4)	324 (2)P	
358 (5)	361 (5)D	361 (0)
428 (3b)	432 (1b)P	
468 (1b)	482 (2b)P	482 (2)
618 (7)	621 (6)D	623 (3)
744 (2)	752 (0b)P	752 (2)
798 (6)	808 (6) P	
812 (6b)	820 (6)P	812 (4)
849 (1)		
991 (1)		
1003 (10)	1008 (12)P	1008 (8)
1031 (8)	1032 (6)P	1032 (2)
1157 (4)	1160 (2) P	
1188 (4)		
1192 (7)	1192 (8)P	1205 (4b)
1414 (5)	1419 (3)P	1416 (0)
1499 (0)		
1589 (5)	1591 (3)P	
1602 (6)	1602 (4)D	1599 (3b)
2252 (6)	2250 (10)P	2249 (6)
2914 (5b)	2920 (10)P	2923 (6)
2984 (3)		
3011 (3)		
3046 (3)		
3059 (9)		
3065 (8b)	3065 (10b)P	3062 (8b)

1956; Biswas, 1956a, 1956b) by triplet→singlet transition, but all disubstituted benzenes do not necessarily produce such luminescence in the visible region. Probably the wavelength of singlet→triplet absorption band of phenyl acetonitrile is longer than 3650 Å group of mercury lines, and in other nitriles not showing such luminescence the absorption band may be at wavelengths shorter than the 3650 Å group.

ACKNOWLEDGMENT

The author is grateful to Professor S. C. Sirkar, D.Sc., F.N.I., for his kind interest and helpful guidance during the progress of the work. The author's thanks are also due to Dr. S. B. Banerjee for his valuable discussions.

REFERENCES

Bishui, B. M., 1948, *Ind. J. Phys.*, **22**, 167.
Biswas, D. C., 1954, *Ind. J. Phys.*, **28**, 423.
Biswas, D. C., 1956a, *Ind. J. Phys.*, **30**, 143.
Biswas, D. C., 1956b, *Ind. J. Phys.*, **30**, 407.
Deb, K. K., 1960, *Ind. J. Phys.*, **34**, 247.
Ferguson *et al.*, 1953, *J. Chem. Phys.*, **21**, 1736.
Kasha, M., 1952, *J. Chem. Phys.*, **20**, 71.
Landolt-Börnstein, 1951, Zahlenwerte und Funktienen, I Band Atom-und Molekular Physik Teil (2), p. 545.
Mukherjee, D. K., 1960, *Ind. J. Phys.*, **34**, 402.
Ray, A. K., 1951, *Ind. J. Phys.*, **25**, 131.
Sanyal, S. B., 1953, *Ind. J. Phys.*, **27**, 447.

3

DYNAMICS OF THE LONGITUDINAL PROPAGATION OF ELASTIC DISTURBANCE THROUGH A MEDIUM EXHIBITING GRADIENT OF ELASTICITY

S. K. GHOSH

Department of Physics, Jadavpur University, Calcutta-32

(*Received July* 6, 1960)

ABSTRACT. Extensional vibration in an isotropic medium for linear variation of elastic parameters has been considered. The problem is worked out following Operational methods. Two distinct cases have been worked from the general solution, namely, (1) for a source having impulsive force at one end, the other end remaining free, and (2), impulsive force at one end, the other end being fixed. Solution obtained in the form of modified Bessel functions have further been simplified for small variations of the parameter using method of steepest descents as adopted by Debye.

INTRODUCTION

The general problem of the extensional vibration of a bar excited by the impact of an elastic load has already been solved for a number of cases by the author, following Operational method. The theory has been further extended to include dynamics of plastic deformations in a bar exhibiting strain-rate effect and subjected to (1) impact stress, (2) alternating stress.

In the present paper, an isotropic elastic medium of uniform density ρ is considered, where the elastic parameters λ, μ, are supposed to vary linearly.

Explanations of the symbols used:

l = Length of the medium

t = Variable time

x = Variable length, measured in the direction of propagation of the disturbance, the medium being free at $x = 0$ and impacted at $x = l$ (as in sec. I). But in section II, the medium is supposed fixed at $x = 0$ and impacted at $x = l$.

U = Displacement at any section.

U_l = Displacement at $x = l$.

ρ = Density of the medium (supposed uniform)

λ, μ = Elastic parameters whose linear variations are supposed in accordance with the relations,

$$\left.\begin{aligned} \lambda &= \lambda_0+\lambda_1 x \\ \mu &= \mu_0+\mu_1 x \end{aligned}\right\} \quad (\lambda_1, \mu_1 > 0)$$

where λ_0, μ_0 are the values at the origin, $x = 0$

v_0 = Velocity of impact.

a_0 = Compressional wave velocity at $x = 0$

J = Impulse per unit area.

P = Pressure of impact.

D = Operator d/dt.

The differential equation governing motion in one dimension in an isotropic elastic medium of uniform density ρ is given by

$$\frac{d}{dx}\left[(\lambda + 2\mu)\frac{du}{dx}\right] = \rho\frac{d^2u}{dt^2} \quad \ldots \quad (1)$$

Using transformation

$$Z = \lambda_0 + 2\mu_0 + (\lambda_1 + 2\mu_1)x \quad \ldots \quad (2)$$

Eq. (1) reduces to

$$Z\frac{d^2u}{dz^2} + \frac{du}{dz} = C^2\frac{d^2u}{dt^2} \quad \ldots \quad (1.1)$$

which is equivalent to

$$Z\frac{d^2u}{dz^2} + \frac{du}{dz} - C^2D^2u = 0 \quad \ldots \quad (1.2)$$

where $$C^2 = \rho/(\lambda_1 + 2\mu_1)^2. \quad \ldots \quad (3)$$

The substitution

$$y = 2CD[\lambda_0 + 2\mu_0 + (\lambda_1 + 2\mu_1)x]^{\frac{1}{2}} \quad \ldots \quad (4)$$

reduces Eq. (1.2) to

$$\frac{d^2u}{dy^2} + \frac{1}{y}\frac{du}{dy} - u = 0 \quad \ldots \quad (1.3)$$

which is modified Bessel's equation of Zero order and has the solution.

$$U(x, t) = AI_0(y) + BK_0(y) \quad \ldots \quad (5)$$

where I_0, K_0 are modified Bessel Functions of zero order.

For large values of y (since C is large for small values of λ_1, μ_1), Eq. (5) can be approximately written, using the method of steepest descents, as adopted by Debye, as

$$U(x, t) = y^{-\frac{1}{2}}[A_1e^{y} + B_1e^{-y}] \quad \ldots \quad (6)$$

SECTION I.

The terminal conditions are :

at the free end $x = 0$, $$\frac{du}{dx} = 0 \qquad \ldots \quad (6.1)$$

and at the end $x = l$, $$u = U_l \qquad \ldots \quad (6.2)$$

Conditions (6.1) and (6.2) reduce equation (6) to

$$U(x, t) = (Z/Z_l)^{-1/4} \cdot \frac{\cosh 2CD(Z^{\frac{1}{2}} - Z_0^{\frac{1}{2}})}{\cosh 2CD(Z_l^{\frac{1}{2}} - Z_0^{\frac{1}{2}})} \cdot U_l \qquad \ldots \quad (7)$$

where
$$\left.\begin{aligned} Z_l &= \lambda_0 + 2\mu_0 + (\lambda_1 + 2\mu_1)l \\ Z_0 &= \lambda_0 + 2\mu_0 \end{aligned}\right\} \qquad \ldots \quad (7.1)$$
and

Now the pressure of impact on the medium at $x = l$ is given by

$$P = -\left(Z \frac{du}{dx} \right)_{x=l} \qquad \ldots \quad (8)$$

An impulse J per unit area is given to the medium, at $x = l$, and the subsequent equation of motion is given by

$$J/v_0 \cdot \frac{d^2U_l}{dt^2} = -\left(Z \frac{du}{dx} \right)_{x=l} \qquad \ldots \quad (9)$$

Now substituting the value of $\left(Z \dfrac{du}{dx} \right)_{x=l}$ as obtained from Eq. (7) in Eq. (9) and imposing the boundary conditions, we have

$$D\rho a_0 \left[1 + \tfrac{1}{2} \frac{(\lambda_1 + 2\mu_1)l}{\lambda_0 + 2\mu_0} \right] U_l \tanh \frac{Dl}{a_0} + J/v_0 \, D^2 U_l = JD. \qquad \ldots \quad (10)$$

retaining up to first power of λ_1, μ_1 and using the condition

$$l < (\lambda_0 + 2\mu_0)/(\lambda_1 + 2\mu_1)$$

Eq. (10) yields,

$$U_l = v_0/F(D). \qquad \ldots \quad (11)$$

where $F(D)$

$$= D + \frac{\rho a_0 v_0}{J}\left\{1+\tfrac{1}{2}\,\frac{(\lambda_1+2\mu_1)l}{\lambda_0+2\mu_0}\right\}\tanh\frac{Dl}{a_0}$$

$$= D+q.\,\frac{1-e^{-2Dl/a_0}}{1+e^{-2Dl/a_0}} \quad \ldots \quad (12)$$

where

$$q = \frac{\rho a_0 v_0}{J}\left\{1+\tfrac{1}{2}\,\frac{(\lambda_1+2\mu_1)l}{\lambda_0+2\mu_0}\right\} \quad \ldots \quad (12.1)$$

Eq. (11) with the help of (12) becomes

$$U_l = \left[\frac{1}{D+q}+\left\{\frac{1}{D+q}-\frac{D-q}{(D+q)^2}\right\}e^{-2Dl/a_0}\right.$$

$$\left.+\left\{\frac{(D-q)^2}{(D+q)^3}-\frac{D-q}{(D+q)^2}\right\}e^{-4Dl/a_0}+\ldots+\ldots\right]v_0$$

$$=[f_1(t)+2f_1(t_1)-2f_2(t_1),+4f_3(t_2)-6f_2(t_2)+2f_1(t_1),+\ldots+\ldots] \quad \ldots \quad (13)$$

where $f(t_n)$ denotes $f(t-n\theta_1)=f(t-n.2l/a_0)$.

The values of the functions are similar to those obtained by the author earlier (Ghosh and Ghosh, 1951).

DISPLACEMENT AT ANY SECTION

Eq. (7) when expanded in terms of its equivalent exponential and simplified using small values of λ_1. μ_1 up to first power gives with the help of Eq. (13),

$$U(x,t) = \left\{1+\frac{1}{4}\,\frac{(\lambda_1+2\mu_1)(l-x)}{\lambda_0+2\lambda_0}\right\}\sum_{r=1}^{n}\left[e^{D/a_0\{x-l-\overline{r-1}.2l\}}\right.$$

$$\left.+\,e^{-D/a_0\{\overline{x-l}+r.2l\}}\right]U_l \quad \ldots \quad (14)$$

where r is an integer.

Eq. (14) is the general form, giving the displacement at any section at any instant during impact.

Now substituting the value of U_l from Eq. (13) in Eq. (14) and collecting only the useful terms occuring during the desired interval of time, we get for the displacement at any section during $0<t<2l/a_0$,

$$U(x,t) = \left\{1+\frac{1}{4}\,\frac{(\lambda_1+2\mu_1)(l-x)}{\lambda+2\mu_0}\right\}\left[e^{\frac{D}{a_0}(x-l)}+e^{-\frac{D}{a_0}(x+l)}\right]f_1(t) \quad \ldots \quad (14.1)$$

$$= \frac{J}{\rho a_0} \left[1 - \frac{1}{4} \frac{(\lambda_1+2\mu_1)(x+l)}{\lambda_0+2\mu_0} \right] \left[1 - e^{-\frac{q}{a_0}(a_0 t - l - x)} \right] \quad \ldots \quad (14.2)$$

Since $a_0 \times v_0$ is large (when v_0 is large), q is large and at $t = l/a_0$ equation (14.2) reduces to

$$U(x, t) = \frac{Jt}{\rho l} \left[1 - \frac{1}{4} \frac{(\lambda_1+2\mu_1)(l+x)}{\lambda_0+2\mu_0} \right] \quad \ldots \quad (14.3)$$

Eq. (14.3) is similar to that obtained by A. N. Dutta (1956) and is a particular case derived from the general solution given by Eq. (14.2).

It is clear that Eq. (14.3) fails to give general displacement $U(x, t)$ for time $t < l/a_0$ *i.e.*, until the waves have reached the far end. Further, the displacement Eq. (13) shows that the wave train does not return after reflection, as shown by the second term of Eq. (15) below.

PRESSURE AT THE IMPACTED END

Combining Eq. (8) with (7), the pressure of impact on the medium at $x = l$, *i.e.* impacted end is numerically given by

$$P = \rho a_0 \left[1 + \frac{1}{2} \frac{(\lambda_1+2\mu_1)l}{\lambda_0+2\mu_0} \right] \tanh \frac{Dl}{a_0} \cdot U'_l$$

$$= \rho a_0 \left[1 + \frac{1}{2} \frac{(\lambda_1+2\mu_1)l}{\lambda_0+2\mu_0} \right] \left[f_1'(t) - 2f_2'(t_1) + 4f_3'(t_2) - 2f_2'(t_2) + \ldots \right] \quad \ldots \quad (15)$$

Thus during $0 < t < 2l/a_0$,

$$P_1 = \rho a_0 \left[1 + \frac{1}{2} \frac{(\lambda_1+2\mu_1)l}{\lambda_0+2\mu_0} \right] \cdot v_0 e^{-qt}. \quad \ldots \quad (15.1)$$

SECTION II

The terminal conditions are:

at the fixed end, $x = 0$, $U = 0$ ... (16.1)

and at the end, $x = l$, $U = U_l$ ... (16.2)

Conditions (16.1) and (16.2) reduce equation (6) to

$$U(x, t) = \left(\frac{Z}{Z_l} \right)^{-1/4} \cdot \frac{\sinh 2CD(Z^{\frac{1}{2}} - Z_0^{\frac{1}{2}})}{\sinh 2CD(Z_l^{\frac{1}{2}} - Z_0^{\frac{1}{2}})} \cdot U_l \quad \ldots \quad (17)$$

Now substituting the value of $\left(Z\frac{du}{dx}\right)_{x=l}$ from Eq. (17) in Eq. (9) and imposing the boundary conditions we have,

$$D\rho a_0\left[1+\frac{1}{\lambda}\frac{(\lambda_1+2\mu_1)l}{\lambda_0+2\mu_0}\right]U_l\coth\frac{Dl}{a_0}+J/v_0\,D^2U_l=JD \qquad \dots \quad (18)$$

retaining up to first power of λ_1, μ_1 and subject to the condition that $l < \frac{\lambda_0+2\mu_0}{\lambda_1+2\mu_1}$

Eq. (18) yields

$$U_l=\frac{v_0}{F(D)} \qquad \dots \quad (19)$$

where
$$F(D)=D+\frac{\rho a_0 v_0}{J}\left\{1+\frac{1}{2}\frac{(\lambda_1+2\mu_1)l}{\lambda_0+2\mu_0}\right\}\coth\frac{Dl}{a_0}$$

$$=D+q\coth\frac{Dl}{a_0} \qquad \dots \quad (20)$$

where
$$q=\frac{\rho a_0 v_0}{J}\left\{1+\frac{1}{2}\frac{(\lambda_1+2\mu_1)l}{\lambda_0+2\mu_0}\right\}\text{ as before.}$$

Eq. (19) with the help of Eq.(20) becomes

$$U_l=f_1(t),+2f_2(t_1)-2f_1(t_1),+4f_3(t_2)-6f_2(t_2)+2f_1(t_2),$$

$$+\dots++2\left[2^{n-1}f_{n+1}(t_n)-2^{n-2}.\frac{n+1}{n}\,{}^nC_1f_n(t_n)+2^{n-3}.\frac{n+2}{n}\,{}^nC_2f_{n-1}(t_n)\right.$$
$$\left.-+\dots+(-1)^nf_1(t_n)\right].$$

The values of the functions are the same as those in Section I.

REFERENCES

Datta, A. N., 1956, *Ind. J. Theo. Phys.*, **4**, No. 2.
Ghosh, M. and Ghosh, S. K., 1951, *Ind. J. Phys.*, **25**, 153.

DISPERSION OF MICROWAVES IN OXYGEN

PREM SWARUP AND S. K. GARG

INSTITUTE OF APPLIED PHYSICS, UNIVERSITY OF ALLAHABAD, ALLAHABAD

(*Received, February* 7, 1960)

ABSTRACT. Dispersion of microwaves has been theoretically calculated in the case of gaseous oxygen on the basis of Van Vleck-Weisskopf expressions for the collision broadened microwave spectral lines. Curves are plotted at pressures of $\frac{1}{4}$, 1, 2, 10, 25 and 50 atmospheres in a wide frequency band both for resonant and nonresonant cases. The calculated value of static magnetic susceptibility agrees with the known experimental value.

INTRODUCTION

Oxygen molecule presents an interesting case in the microwave region. The molecule is electrically nonpolar and the absorption and dispersion of microwaves is attributed to it being magnetically polar. Analysis of the band spectrum has shown that oxygen molecule has a $^3\Sigma$ ground state. It has the spin quantum number unity and the Lande g factor two and, hence, the molecule has the magnetic dipole moment of 2 Bohr magnetons ; which interacts with the 'end over end' rotation of the molecule to form a 'rho type triplet'. The resolved fine structure of the microwave spectrum has been studied by a number of workers in the vicinity of 60 kMcps.[1,2]. The transitions involved here are between $J = K$ and $J = K-1$ (negative transition) and $J = K$ and $J = K+1$ (positive transitions). Selection rule prohibits the transition between $J = K-1$ and $J = K+1$. These states nearly coincide and differ from $J = K$ by about 2 cm^{-1} and hence all the lines are clustered about 2 cm^{-1}. There is, however, a subsidiary resonance at 4 cm^{-1} involving the single transition $J = K$ to $J = K-1$ for $K = 1$. In addition to this resonance absorption, oxygen molecule also shows a nonresonant or Debye type of absorption and dispersion which is attributed to the diagonal part of the matrix element of the magnetic moment i.e. projection of the Spin vector S parallel to the resultant angular moment vector J about which S precesses. On the average it is found that one third of the total mean squared moment is of the diagonal variety while the other two third being consumed by the nondiagonal type of absorption i.e. the resonance absorption. The study of the resolved oxygen spectrum in the low pressure has shown about 29 absorption lines. The measurement of the line width parameter (Artman, 1953) has shown that it is very nearly constant for all the lines. At a higher pressure, all the lines merge to form a single broad line with centroid frequency at 2 cm^{-1}. An average value of the line width parameter weighted for line intensity has been found to

be 1.94 Mc/mm Hg. In case of air, allowing for difference in collision cross section between oxygen and air, the average value is 18% lower i.e. 0.039 cm^{-1}/atm. The value of the line width parameter for the 'nonresonant' line at zero frequency is still uncertain for lack of any experimental absorption data at wavelengths above 1 cm. Van Vleck (1947) predicted the attenuation offered by oxygen in the millimeter region due to the nonresonant line taking two likely values of the line width parameter i.e. $\overline{\Delta\nu} = 0.02$ and 0.05 cm^{-1}/atmos. the former being the most probable value and the latter being the upper limit.

CALCULATIONS

Van Vleck's and later Artman's calculations predicting the amount of attenuation offered by oxygen in the mm region at atmospheric pressure of air were based on the quantum mechanical expressions of VanVleck and Weisskopf (1945) for the collision broadened microwave spectral lines. The expression for the absorption coefficient is:

$$\frac{\alpha'}{\bar{\nu}^2} = \frac{4\pi^2 \Sigma N_{ij}|\mu_{ij}|^2}{3kT}\left[\frac{\overline{\Delta\nu}^2}{\overline{\Delta\nu}^2+(\bar{\nu}+\bar{\nu}_0)^2}+\frac{\overline{\Delta\nu}^2}{\overline{\Delta\nu}^2+(\bar{\nu}-\bar{\nu}_0)^2}\right] \quad \ldots (1)$$

$$= 2\pi I.p\left[\frac{\overline{\Delta\nu}^2}{\overline{\Delta\nu}^2+(\bar{\nu}+\bar{\nu}_0)^2}+\frac{\overline{\Delta\nu}^2}{\overline{\Delta\nu}^2+(\bar{\nu}-\bar{\nu}_0)^2}\right] \quad \ldots (2)$$

where α is the absorption coefficient (per cm); $\bar{\nu}$ is the frequency (cm^{-1}); $\bar{\nu}_0$ is the resonance frequency ; $\overline{\Delta\nu}$ is the line width parameter (cm^{-1}) ; I is the intensity factor and p is the pressure in cm of Hg.

The contribution of the nonresonant line with the line width parameter $\overline{\Delta\nu_0}$ to the absorption at a frequency $\bar{\nu}$ is obtained by putting $\bar{\nu}_0 = 0$ and using half the value of $I.p$, since one third of the squared moment contributes to the nonresonant absorption while two thirds to the resonant absorption, in the expression (2) above:

$$\frac{\alpha''}{\bar{\nu}^2} = 2\pi\left(\frac{I.p}{2}\right)\left[\frac{2\overline{\Delta\nu}^2_0}{\overline{\Delta\nu}^2_0+\bar{\nu}^2}\right] \quad \ldots (3)$$

$$= 2\pi \; I.p[\overline{\Delta\nu}^2_0/(\overline{\Delta\nu}^2_0+\bar{\nu}^2)]$$

Hence the net absorption at a frequency comes out to be:

$$\frac{\alpha}{\bar{\nu}^2} = \frac{\alpha'+\alpha''}{\bar{\nu}^2} = 2\pi I.p\left[\frac{\overline{\Delta\nu}^2}{\overline{\Delta\nu}^2+(\bar{\nu}+\bar{\nu}_0)^2}+\frac{\overline{\Delta\nu}^2}{\overline{\Delta\nu}^2+(\bar{\nu}-\bar{\nu}_0)^2}+\frac{\overline{\Delta\nu_0}^2}{\overline{\Delta\nu_0}+\nu^2}\right] \ldots (4)$$

The associated dispersion of the microwaves due to the magnetic dipole moment can be calculated by the quantum mechanical Van Vleck-Weisskopf expression

for dispersion. The case is parallel to the calculation of the electric susceptibility in ND_3 by the author (1956). In this case the magnetic susceptibility $(\mu'-1)$ or δ_m at a frequency $\bar{\nu}$ due to a resonance line at $\bar{\nu}_0$ of line width parameter $\overline{\Delta\nu}$

$$\delta_m'' = I.p \left[\frac{\overline{\Delta\nu}^2+\bar{\nu}_0(\bar{\nu}+\bar{\nu}_0)}{\overline{\Delta\nu}^2+(\bar{\nu}+\bar{\nu}_0)^2} + \frac{\overline{\Delta\nu}^2-\bar{\nu}_0(\bar{\nu}-\bar{\nu}_0)}{\overline{\Delta\nu}^2+(\bar{\nu}-\bar{\nu}_0)^2} \right] \quad \ldots (5)$$

$$= I.p.S \quad \ldots (6)$$

where S is the shape function. The expression for the contribution of the Debye line at zero frequency to the net susceptibility at a frequency $\bar{\nu}(\text{cm}^{-1})$ with the line width parameter $\overline{\Delta\nu_0}$ is obtained by putting $\bar{\nu}_0 = 0$ and taking half the value of $I.p.$in the expression (5) above. The expression is:

$$\delta_m' = \frac{I.p}{2} \left[\frac{2\overline{\Delta\nu_0}^2}{\overline{\Delta\nu_0}^2+\bar{\nu}^2} \right] \quad \ldots (7)$$

Hence the net value of the magnetic susceptibility at a frequency $\bar{\nu}$ taking into account the contributions of the nonresonant and resonant lines is:

$$\delta_m = \delta'_m+\delta''_m = I.P. \left[\frac{\overline{\Delta\nu}^2+\bar{\nu}_0(\bar{\nu}+\bar{\nu}_0)}{\overline{\Delta\nu}^2+(\bar{\nu}+\bar{\nu}_0)^2} + \frac{\overline{\Delta\nu}^2-\bar{\nu}(\bar{\nu}_0-\bar{\nu}_0)}{\overline{\Delta\nu}^2+(\bar{\nu}-\bar{\nu}_0)^2} + \frac{\overline{\Delta\nu}^2_0}{\overline{\Delta\nu}^2+\bar{\nu}^2_0} \right] \ldots (8)$$

The values of $I.p.$ have been calculated at different pressures (Maryott and Birnbam, 1955) and tabulated in Table I.

TABLE I

Values of intensity factor at different pressures and at 20°C

	Pressure in Atmospheres			
	1	2	25	50
$I.p \times 10^6$	0.59	1.19	14.89	29.77

DISPERSION NEAR 2CM-1

The dispersion curves have been calculated for the individual lines at $\frac{1}{4}$ atmospheric pressure where most of the lines are resolved and for the pressure broadened envelope at higher pressures. The value of the line width parameter has been taken to be 1.94 Mc/mm Hg and its variation with pressure has been assumed to be linear. Table II gives the various frequencies of transitions (Artman 1953 and Burkhalter *et al.*, 1950) together with their relative intensities. The intensities have been calculated by the following formulae:

$$(I.\overline{\Delta\nu})_- = 2.917\times10^{-14}\ \frac{(\upsilon_{k-})^2(K+1)(2K-1)}{T^3\qquad K} \exp\left[-\frac{2.072K(K+1)}{T}\right] \frac{10^{-6}\text{cm}^{-1}\ MC}{\text{mm}Hg}$$

$$(I.\bar{\Delta}\nu)_+ = 2.917\times 10^{-14}\ \frac{(\nu_{k+})^2}{T^3}\ \frac{K(2K+3)}{K+1}\ \exp\left[-\frac{2.072K(K+1)}{T}\right].\ \frac{10^{-6}\text{cm}^{-1}MC}{\text{mm Hg}}$$

The value of $(I.\bar{\Delta}\nu)$ for the most intense transition $J = 9$ to $J = 10$ is 41.01×10^{-6} cm^{-1} Mc/mm Hg. Fig. 1 shows the complex dispersion pattern calculated at

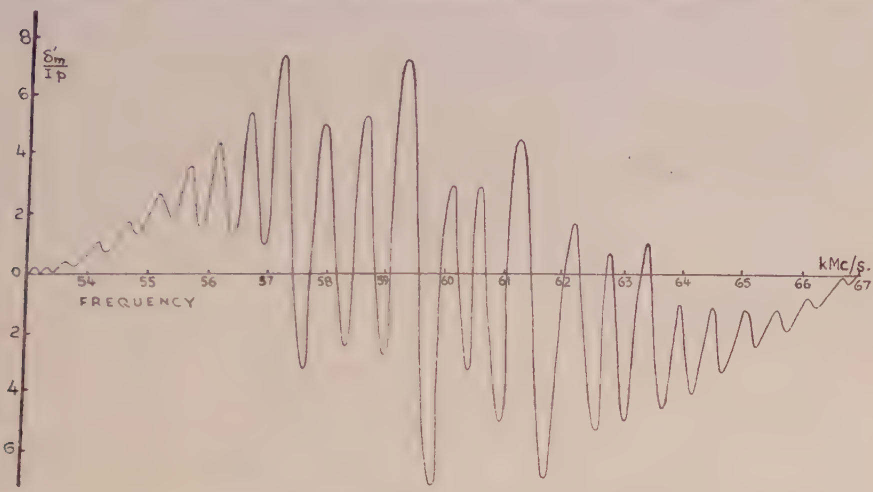

Fig. 1. Dispersion curves of oxygen at .25 atmospheric pressure in the 2 cm^{-1} region.

a pressure of $\frac{1}{4}$ atmosphere for individual lines and then added up for all the lines. The relative intensities of the absorption lines are given in Table II. The lines lose their individuality at higher pressures and hence the curves drawn in Fig. 2 at pressures of 1. 10, 25, 50 atmosphere show single broad dispersion curves due

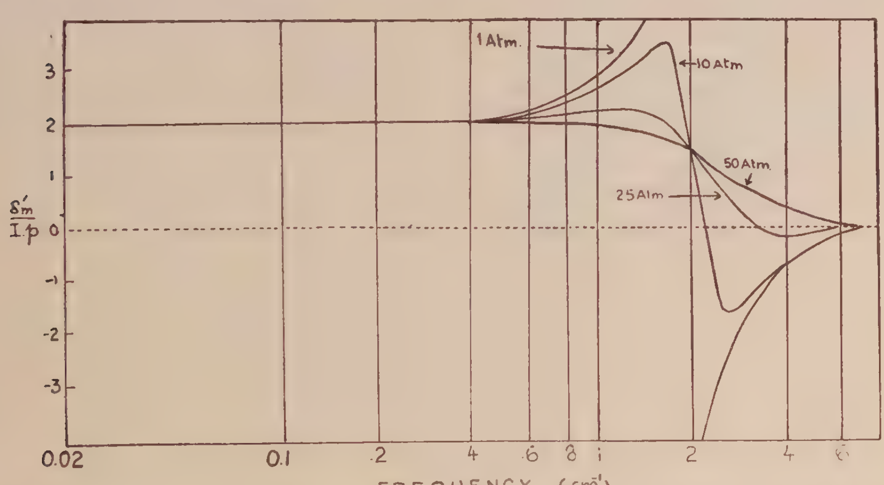

Fig. 2. Dispersion curves of oxygen at 1,10,25 and 50 atmospheric pressure in the wide frequency band due to the resonance line at 2 cm^{-1}.

to the envelope. It is observed that in case of oxygen low pressure conditions prevail even at one atmosphere pressure because of its small collision diameter ($\sim$ 4 Å) as compared to the average distance between the molecules ($\sim$30 Å).

TABLE II

K	Negative transitions $J = K \rightarrow J = K-1$ Frequency	Intensity	Positive transitions $J = K \rightarrow J = K+1$ Frequency	Intensity
1	118.750 kMc/s	0.732	56.265 kMc/s	0.205
3	62.486	0.631	58.446	0.560
5	60.306	0.840	59.592	0.823
7	59.163	0.930	60.435	0.972
9	58.324	0.909	61.152	1.000
11	57.612	0.804	61.800	0.926
13	56.969	0.654	62.412	0.796
15	56.363	0.492	62.998	0.616
17	55.784	0.348	63.568	0.447
19	55.221	0.226	64.128	0.356
21	54.673	0.139	64.679	0.194
23	54.130	0.080	65.223	0.116
25	53.592	0.043	65.762	0.065
27	53.066	0.022	66.296	0.034
29	×		66.828	0.017

DEBYE DISPERSION

Contribution to the magnetic susceptibility of the gas by the diagonal component of the matrix element magnetic dipole moment has been calculated on the basis of expression (7). Since the exact value of $\overline{\Delta\nu_0}$ is still not known, dispersion curves are plotted in Fig. 3 for the value of $\Delta\nu_0 = 0.02$ cm^{-1}/atmosphere at pressures of 1, 2, 20 and 50 atmospheres. The dispersion is very sharp at low pressures and as the pressure is increased, it broadens and extends to the higher frequency region.

The net value of the magnetic susceptibility of the gas can be obtained by adding the two component values from the graphs or calculating it from the general

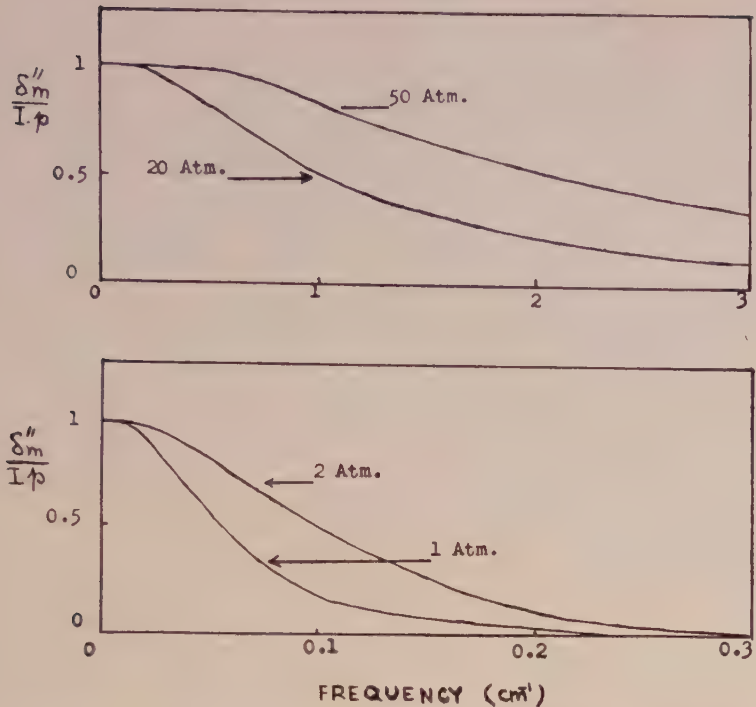

Fig. 3. Dispersion curves of oxygen at 1, 2,20 and 50 atmospheric pressure in the wide frequency band due to the nonresonant or Debye line at zero frequency.

expression (8). The value of static magnetic susceptibility at one atmospheric pressure and 20°C comes out to be :

$$(\mu'-1)_0 = \delta'_{m0}+\delta''_{n0}$$
$$= 3\, I.p = 1.78\times10^{-6}.$$

This value compares very well with the value of $(\mu'-1)$ as 1.8×10^{-6} quoted by Birnbaum *et al* (1951). More experimental work specially at higher wavelengths is needed in this direction.

RFERENCES

Artman, J. O., 1953 Columbia Rad. Lab. Report, June 1.

Birnbaum, G., S. J. Kryder and H. Lyons, 1951, *J. Appl. Phys.*, **22**, 95.

J. H. Burkhalter, R. S. Anderson, W. V. Smith and W. Gordy, 1950, *Phys. Rev.* **79**, 651.

Maryott, A. A. and Birnbaum, 1955, G., *Phys. Rev.*, **99**, 1886.

Prem Swarup, 1956, *Phys. Rev.*, **104**, 89.

Townes, C. H. and Schawlow, A. L. 1955, Microwave Spectroscopy (McGraw Hill).

Van Vleck, J. H., 1947, *Phys. Rev.*, **71**, 413.

Van Vleck, J. H. and Weisskopf, V. F., 1945, *Rev. Mod. Phys.*, **17**, 227.

5

A MINIMISATION METHOD OF BOOLEAN FUNCTIONS

AMARENDRA MUKHOPADHYAY

INSTITUTE OF RADIO PHYSICS AND ELECTRONICS,

UNIVERSITY OF CALCUTTA

(*Received June* 10, 1960)

ABSTRACT. Algebraic, graphical, chart and numerical methods of minimisation of Boolean Functions have been proposed by several authors (Karnaugh, 1953; McClusky 1956; Shannon, 1938; staff of Harvard computation laboratory, 1951 and Troye, 1959). These methods aim at improving the design of switching circuits which are extensively employed now a days in digital equipments. In the present paper we shall put forward a method of minimisation which has been developed by a combination of the principles underlying the methods of Svoboda and McClusky. In particular, a procedure has been suggested which reduces to a great extent the number of trial-repetitions required to minimise functions which form into a cyclic basic cell chart.

INTRODUCTION

(a) *The minimal form*

Functions of Boolean variables, like the variables themselves, express the states of binary quantities. The function can have only two values 1 or 0, corresponding to the presence or absence of a particular state. A convenient way of describing the function is to specify in a table the value of the function for each combination of input conditions, such as shown in Table 1, for a three variable function $f(x_1, x_2, x_3)$.

TABLE I

x_1	x_2	x_3	f	Minterms	Decimal equivalent values of minterms
0	0	0	1	$x'_1x'_2x'_3$	0
0	0	1	0	$x'_1x'_2x_3$	1
0	1	0	0	$x'_1x_2x'_3$	2
0	1	1	1	$x'_1x_2x_3$	3
1	0	0	1	$x_1x'_2x'_3$	4
1	0	1	0	$x_1x'_2x_3$	5
1	1	0	0	$x_1x_2x'_3$	6
1	1	1	1	$x_1x_2x_3$	7

In canonical form, f can be expressed as

$$f = x'_1x'_2x'_3 + x'_1x_2x_3 + x_1x'_2x'_3 + x_1x_2x_3$$
$$= \Sigma\,(0, 3, 4, 7)[\text{decimal mode of writing } f]$$

The expression for f derived from the truth table, called the canonical expansion of f, can be written in several reduced forms by applying few theorems of Boolean Algebra. But when the function becomes complex, algebraic manipulation is not very helpful and we resort to special methods.

Of all the alternative expressions for f, we call one (and sometimes more than one) the "minimal form" which involves a minimum number of total operations. The number of operations equals the sum total of "Boolean product" operations to realise the reduced minterms and the "Boolean sum" operations to realise the expansion. It follows from this definition that a minimum of diode circuit elements will be required for physical realisation of the function expressed in the minimal form.

(b) *Neighbours, cells and weight*

The terms of the canonical form of a given n-variable Boolean function can be depicted by nodes of an n-dimensional cube. A single variable is depicted by two modes connected by a line. With two variables (x_1, x_2) we require four nodes connected by four lines. When there are n variables, we take $(n+1)$ vertical dotted line, and number then 0, 1, 2, ... n from left. We construct n_{c_0}, n_{c_1}, ... n_{cn} number of nodes over each of these lines respectively and name the nodes with binary numbers having no '1', one '1', two '1's, and so on up to n '1's, i.e. having index values $r = 0, 1, 2 \ldots, n$, over the $(n+1)$ vertical lines. These are then arranged from top to bottom over any line having increasing decimal equivalent value. Lines are then drawn between nodes which differ in exactly one variable and no line is drawn further. The vertices of the cube represent all possible minterms of the canonical expansion and the cube can be considered to be made up of cells (Urbano and Mueller, 1956).

0-cell or vertex	-a point	$k = 0$
1-cell	-a line	$k = 1$
2-cell	-quadrilateral	$k = 2$
3-cell	-hexahedron	$k = 3$
k-cell		$k = k$

where k denotes the order of the cells.

The nodes or vertices which are joined to a particular node or vertex, are called the neighbours or adjacent states of the vertex. The total number of

neighbours belonging to the body of the specified Boolean function with reference to a particular vertex is called the weight of the vertex, and this equals to the number of 1-cells incident with the vertex.

To illustrate the above terms let us take the function expressed in canonical form as

$$f(x_5, x_4, x_3, x_2, x_1, x_0) = \Sigma\,(0, 1, 3, 5, 7, 8, 10, 12, 15, 16, 17, 21, 24, 26, 28, 29, 30, 32, 33, 34, 35, 37, 39, 40, 42, 45, 46, 49, 50, 54, 55, 58, 59, 60, 61, 62, 63) \quad \ldots \quad (1)$$

We shall find all the cells incident with each vertex and also the weights of the vertices.

The above is a six-variable function. In Svoboda's method the function is first projected in a modified Veitch diagram. The different cells are found by using six contact grids and the weight of each vertex is found by using six directional grids (Svoboda, 1956 and Choudhury, 1959). Following McClusky (McClusky, 1956) we shall adopt a method in which the ideas of cells and weight can be directly incorporated and which can be easily extended to cover cases involving more than six variables.

To start with Table II is prepared as follows:

The decimal numbers corresponding to the vertices of the given function [Eq. (1)] are entered in column (a) in groups (indicated by separations) having increasing index values viz., $r = 0, 1, \ldots 6$.

The combinations entered in column (b) are selected from column (a) taking two numbers having index values r and $r+1$ respectively when

$$M_{r+1} - N_r = 2^k \quad \ldots \quad (2)$$

where $k = 0, 1, 2 \ldots$ and M_{r+1}, N_r are numbers belonging to the groups having index values $r+1$ and r respectively. The terms in column (b) will then show all possible 1-cells present in the given function. The difference expressed by Eq.(2) is entered within brackets. Thus 1 and 3 form a 1-cell, but 1 and 10 will not form a 1-cell.

The combinations in column (c) are derived from column (b), taking two terms from any two consecutive groups (i.e. on two sides of a separation line) when their first difference (Eq.(2)] tally and the second difference between leading numbers is again positive and equals 2^k, $(k = 0, 1, 2, \ldots)$, these differences being indicated in brackets. The terms in this column show all possible 2-cells present in the given function. We need only enter cells whose vertices form an increasing sequence of decimal numbers.

Similarly, column (d) has been prepared from column (c) when both the first and second differences tally and the third difference between leading numbers is again 2^k. The term in column (d) shows the only 3-cell present in the function.

Check marks are placed at any stage of combination when cells of a given k-value combine to form a cell of next higher order. We also check mark the cells which will give rise to alternative modes of formation of any higher order k-cell. Thus 1-cells 0, 1 (1) and 16, 17 (1) and also 0, 16 (16) and 1, 17 (16) are check marked since they form the 2-cell 0, 1, 16, 17 (1, 16). The unchecked cells are called the basic cells or the prime implicants of the given function.

Column (b) of Table II contains all information about the neighbours and weight of each vertex. The number of times a given vertex combine in this column is equal to its weight and the companions are its neighbours. Thus the vertex 1 has neighbour 0 in the top group and 3, 5, 17, 33 in the group just below the top, and we need not look down the column after the 1-cell 1, 33 (32), because 1 can never occur below this term. Hence weight of 1 is 5. Thus one can quickly compute the weight of each vertex, and find its neighbours, as listed in Table III.

THE MINIMISATION METHOD

The determination of minimum sum essentially consists of selecting a minimum number of basic cells so that their sum gives the specified output for all combinations of input variables.

TABLE II

Determination of cells

	(a) ✓	(b) ✓	(c)	(d)
$r = 0$	0 ✓	0,1(1) ✓	0,1,16,17(1,16)—*W*	1,3,5,7,33,35,37,39(2,4,32)—*A*
	1 ✓	0,8(8) ✓	0,1,32,33(1,32)—*V*	
	8 ✓	0,16(16) ✓	0,8,16,24(8,16)—*U*	
$r = 1$	16 ✓	0,32(32) ✓	0,8,32,40,(8,32)—*T*	
	32 ✓	1, 3(2) ✓	1,3,33,35,(2,32) ✓	
	3 ✓	1, 5(4) ✓	1,3,5, 7,(2,4) ✓	
	5 ✓	1,17(16) ✓	1,5,17,21(4,16)—*S*	
	10 ✓	1,33(32) ✓	1,5,33,37(4,32) ✓	
	12 ✓	8,10(2) ✓	1,17,33,49(16,32)—*R*	
$r = 2$	17 ✓	8,12(4) ✓	8,10,24,26(2,16)—*Q*	
	24 ✓	8,24(16) ✓	8,10,40,42(2,32)—*P*	
	33 ✓	8,40(32) ✓	8,12,24,28(4,16)—*O*	
	34 ✓	16,17(1) ✓	32,33,34,35(1,2)—*N*	
	40 ✓	16,24(8) ✓	32,34,40,42(2,8)—*M*	
	7 ✓	32,33(1) ✓	3,7,35,39(4,32)	
	21 ✓	32,34(2) ✓	5,7,37,39(2,32)	
	26 ✓	32,40(8) ✓	10,26,42,58(16,32)—*L*	

TABLE II—(*contd.*)

Determination of cells

	(*a*) √	(*b*) √	(*c*)	(*d*)
$r = 3$	28 √	3,7(4) √	24,26,28,30(2,4)—*K*	
	35 √	3,35(32) √	33,35,37,39(2,4) √	
	37 √	5,7(2) √	34,42,50,58(8,16)—*J*	
	42 √	5,21(16) √	26,30,58,62(4,32)—*I*	
	49 √	5,37(32) √	28,29,60,61(1,32)—*H*	
	50 √	10,26(16) √	28,30,60,62(2,32)—*G*	
	15 √	10,42(32) √	42,46,58,62(4,16)—*F*	
	29 √	12,28(16) √	50,54,58,62(4,8)—*E*	
	30 √	17,21(4) √	54,55,62,63(1,8)—*D*	
	39 √	17,49(32) √	58,59,62,63(1,4)—*C*	
$r = 4$	45 √	24,26(2) √	60,61,62,63(1,2)—*B*	
	46 √	24,28(4) √		
	54 √	33,35(2) √		
	58 √	33,37(4) √		
	60 √	33,49(16) √		
	55 √	34,35(1) √		
$r = 5$	59 √	34,42(8) √		
	61 √	34,50(16) √		
	62 √	40,42(2) √		
$r = 6$	63 √	7,15(8)—*b*		
		7,39(32) √		
		21,29(8)—*a*		
		26,30(4) √		
		26,58(32) √		
		28,29(1) √		
		28,30(2) √		
		28,60(32) √		
		35,39(4) √		
		37,39(2) √		
		37,45(8)—*Z*		
		42,46(4) √		
		42,58(16) √		
		50,54(4) √		
		50,58(8) √		
		29,61(32) √		
		30,62(32) √		
		39,55(16)—*Y*		
		45,61(16)—*X*		
		46,62(16) √		
		54,55(1) √		
		54,62(8) √		
		58,59(1) √		
		58,62(4) √		
		60,61(1) √		
		60,62(2) √		
		55,63(8) √		
		59,63(4) √		
		61,63(2) √		
		62,63(1) √		

TABLE III

Determination of weight and neighbours

Vertex	Neighbours	Weight
0	1, 8, 16, 32	4
1	0, 3, 5, 17, 33	5
8	0, 10, 12, 24, 40	5
16	0, 24, 17	3
32	0, 33, 34, 40	4
3	1, 7, 35	3
5	1, 7, 21, 37	4
10	8, 26, 42	3
12	8, 28	2
17	1, 16, 21, 49	4
24	8, 16, 26, 28	4
33	1, 32, 35, 37, 49	5
34	32, 35, 42, 50	4
40	8, 32, 42	3
7	3, 5, 15, 39	4
21	5, 17, 29	3
26	10, 24, 30, 58	4
28	12, 24, 29, 30, 60	5
35	3, 33, 34, 39	4
37	5, 33, 39, 45	4
42	10, 34, 40, 46, 58	5
49	17, 33	2
50	34, 54, 58	3
15	7	1
29	21, 28, 61	3
30	26, 28, 62	3
39	7, 35, 37, 55	4
45	37, 61	2
46	42, 62	2
54	50, 55, 62	3
58	26, 42, 50, 59, 62	5
60	28, 61, 62	3
55	39, 54, 63	3
59	58, 63	2
61	29, 45, 60, 63	4
62	30, 46, 54, 58, 60, 63	6
63	55, 59, 61, 62	4

McClusky's method consists essentially of drawing a prime implicant table, selecting the basis rows, then ruling out each row which is covered by another. The first step is now repeated and the procedure continued until all the states are included or a cyclic prime implicant chart results. Then a trial repetition process is followed to obtain the minimal sum.

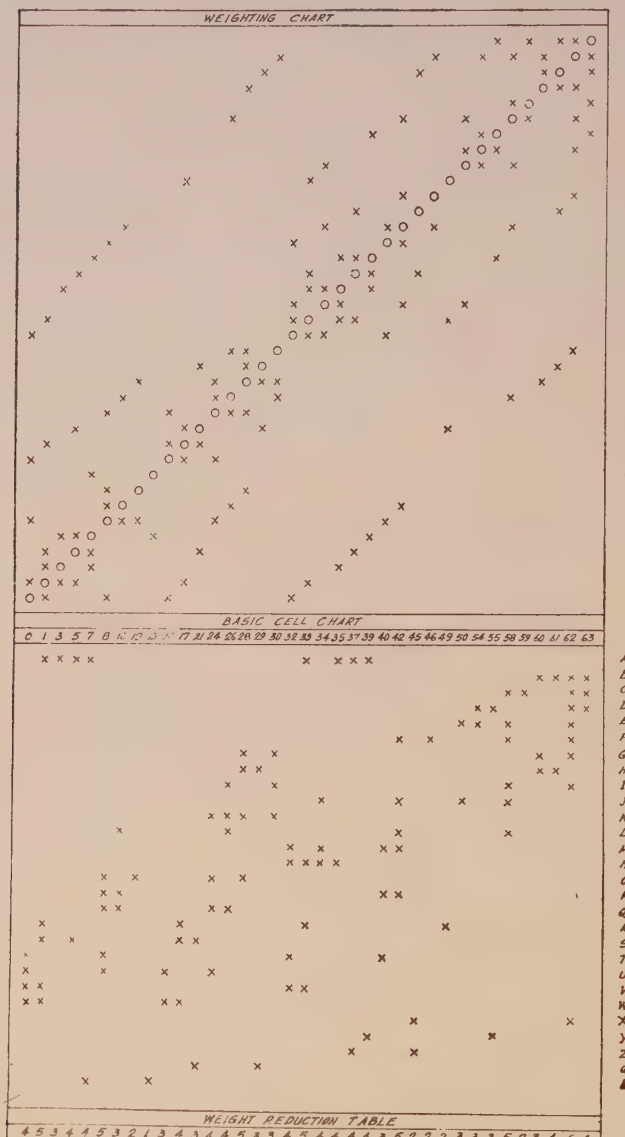

Fig. 1. The basic-cell chart, the weighting chart and the weight reduction table for the function expressed by Eqn. (1).

Svoboda follows a few methodical steps realised by applying the contact grids and directional grids on a modified Veitch diagram. We shall adapt these steps to McClusky's chart, with some obvious advantages. The method may be illustrated by taking the example of minimising the function given in Eq. (1).

A basic cell chart, which is what McClusky calls "the prime implicant table", is first drawn (Fig. 1). The columns carry at their heads the decimal numbers corresponding to all the vertices which are contained in the expression of the function and the horizontal rows correspond to basic cells. The vertices which combine to form a basic cell are cross-marked at the intersections with the horizontal row representing the particular basic cell. Thus the basic cell Z has been formed by combining 1, 3, 5, 7, 33, 35, 37, 39 and crosses in the A row are placed under these columns only and so on for all other rows.

We shall now introduce one new chart and a table. Over the basic cell chart, a weighting chart is placed which depicts all the neighbours of each vertex and hence determines the weight of the latter. This chart is drawn from the data in Table III or directly from column (b) of Table II or, if anybody prefers, with the help of a Karnaugh map. Small circles are entered over each of the vertex of the given function in successive horizontal lines so that the circles are located over a diagonal line. Crosses entered in the horizontal line are the neighbours of the vertex represented by the circle in that horizontal line. Thus, crosses corresponding to 1, 8, 16, 32, are the neighbours of the circle representing the vertex 0. The weighting chart has the interesting property that it is symmetrical about the diagonal line.

Below the basic cell chart, a weight reduction table is formed. In the first row of this table, weights of all vertices computed from the weighting chart are entered under corresponding columns.

We shall now proceed to utilise Svoboda's methodical steps (Svoboda, private communication) to obtain the minimal form.

FIRST STEP

The terms which are essential for inclusion in all possible minimal forms satisfy the theorem:

"Theorem I: The sufficient condition for inclusion of a term T in (any of) the minimal forms of the function is the incidence of the corresponding k-cell t with a vertex V of weight k".

We begin with cells having smallest weight. If the weight of a vertex is zero or one, one always obtains a term satisfying the above condition. In Fig. 3 there is no vertex with weight $k = 0$. The vertex 15 has weight $k = 1$ and there is the 1-cell b(7, 15) in row (b), which therefore is an essential term. Again, the vertices 12, 46, 49, 59 have weights $k = 2$, and to each of them is incident one

2-cell in the rows 0(8, 12, 24, 28), F(42, 46, 58, 62), R(1, 17, 33, 49) and C(58, 59, 62, 63) respectively, and hence they represent essential cells. But with the vertex 45 having weight $k = 2$, there is no 2-cell incident and hence there is no essential term corresponding to this vertex. The vertex 3 has weight $k = 3$ and there is a 3-cell incident with this in the row A(1, 3, 5, 7, 33, 35, 37, 39), which is therefore essential. No other vertex of weight $k = 3$ satisfies the sufficient condition of

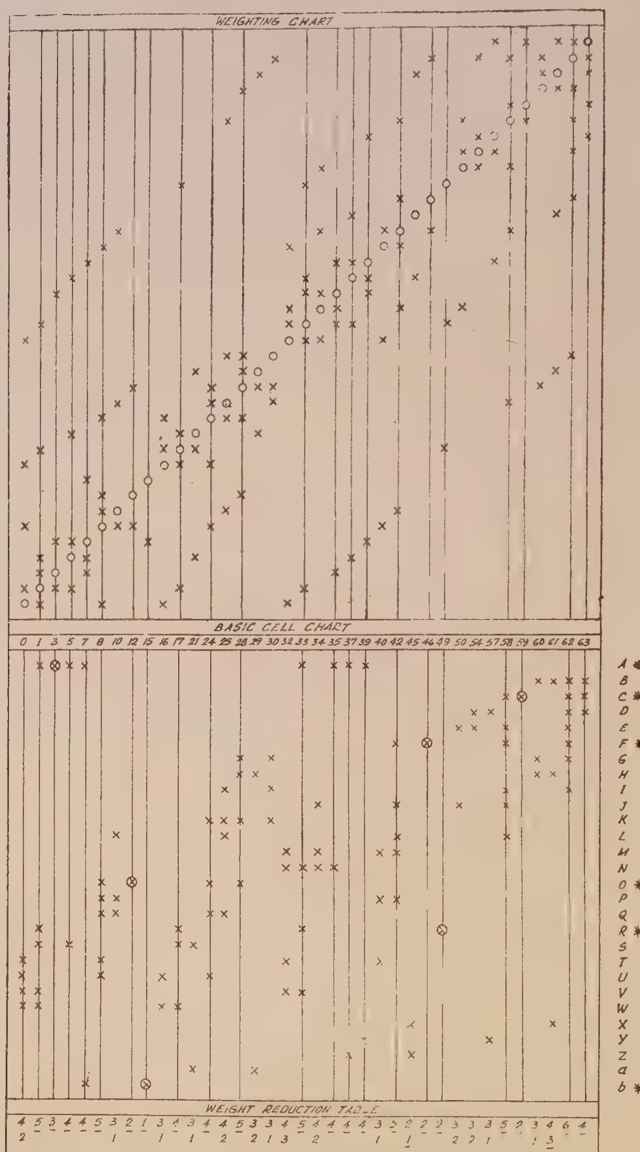

Fig. 2. The form of the charts after the first methodic step.

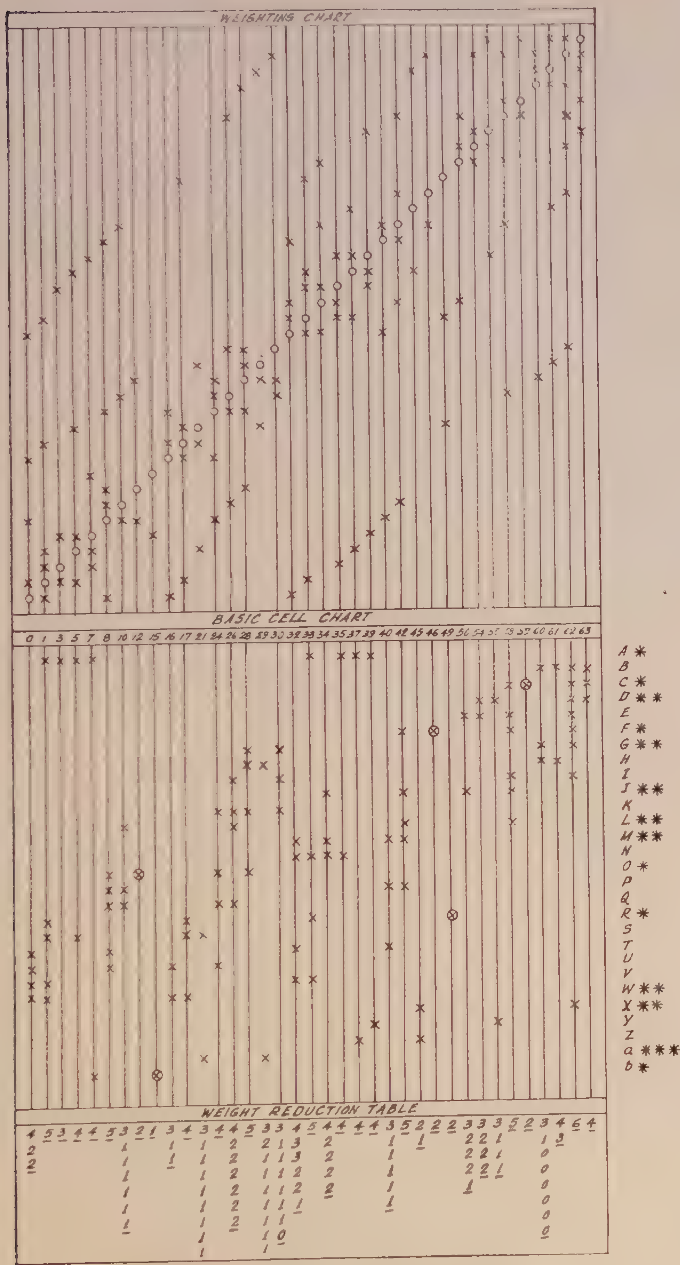

Fig. 3. The form of the charts after the second methodic step.

Theorem I. We do not require to look into the vertices of weights $k = 4, 5, 6$, since it is evident from Table II, that for the function in question, there is no cell of order 4, 5, or 6.

Thus, by the first methodic step we have selected rows A, C, F, O, R, b, marked by asterisk at the extreme right of the rows (Fig. 2). It is interesting to note that this step is identical with the first step in McClusky's method e.g., finding the columns which contain only one cross and selecting the rows as the basis rows in which these crosses occur.

All the columns in which the essential rows have entries are lined out, because the vertices corresponding to these columns have become bound to the chosen configuration of cells in the first step. The lining out is also extended to the weighting chart so that the free neighbours of the free vertices become apparent (see Fig. 2).

Definition : The free weight W of a vertex V_0 is equal to the number of 1-cells belonging to the body of the Boolean function incident with the vertex V_0 and incident with W free vertices $V_1, V_2 \ldots V_W$. The vertices $V_1, V_2 \ldots V_W$ are called free neighbours of the vertex V_0.

The reduced or the free weights of free vertices are now easily computed by counting the number of unruled crosses occurring in the horizontal line for any vertex. Thus for the free vertex 0, we find the number of unruled crosses is equal to 2 corresponding to the free neighbours 16 and 32. Hence the reduced weight of the vertex is 2. The weighting chart, therefore, not only enables to compute the reduced weight, but also shows which neighbours of a particular vertex are still free.

The reduced weight of each free vertex is computed and entered in the second row of the weighting table, under corresponding columns of the vertices. Each of the vertices which is bound in the first step is marked in this table by putting a bar under the number representing its weight. The appearance of the charts is shown in Fig. 2.

SECOND STEP

The second step is to select those terms which might be included in at least one of the minimal forms. For this we utilise the theorem :

Theorem II : A sufficient condition for a term T_{n+1} to be included in at least one of the minimal forms is satisfied when all the following propositions are true :

(1) The partial form $F_n = T_1 + T_2 + \ldots + T_n$ (corresponding to the body of all bound vertices built from cells $t_1, t_2 \ldots t_n$) has been included in one of the minimal forms.

(2) There is a K-cell t_{n+1} incident with a free vertex V_0, with all free neighbours $V_1, V_2 \ldots V_W$, with free vertices $V_{W+1}, V_{W+2}, \ldots V_{W+p}$ and with any number of bound vertices ($W \leqslant K$ being the free weight of the vertex V_0).

(3) There is no k-cell incident with the V_0 and with another free vertex not belonging to the set $V_0, V_1 \ldots V_{W+p}$.

(4) All k-cells incident with V_0 have $k \leqslant K$.

(5) The term T_{n+1} corresponds to the K-cell t_{n+1}

In Fig. 4, the free vertex 45 has free weight $W = 1$. It will be seen that there is a K-cell $X(45, 61)$ satisfying the sufficient conditions of Theorem II. Columns 45 and 61 are lined out and the lining out is extended to the weighting chart.

Fig. 4. Selection of cell A in the problem of minimising the function expressed in Eq. (iv).

Now, due to ruling out 61, weights of 60 and 29 are reduced further by unity. The weights for other free vertices remain unchanged. The free-weights are now written in the third row of the weighting table (Fig. 3).

The vertex 60 has free weight $W = 0$, but no cell incident on it (e.g., B, G, H)satisfies the sufficient condition of Theorem II, because with B, the vertex 30 of G or vertex 29 of H are not covered. Similar arguments apply to cells G or H. From the vertices having free weight $W = 1$, are incident 2-cells U and W with 16; both of these take all the free neighbours—here 0 only—of 16. Also $K = 2 > W = 1$; all k -cells have $k = K$, so that we can take either. But for vertex 10, cell L takes its only free neighbour 26, but there is a cell P incident with 10 containing the vertex 40 which is not included in cell L; hence L cannot be included. The vertex 21 has $W = 1$. The cell 'a' incident with 21 takes its only neighbour 29, its $K = 1 = W$, but there is a k-cell S having $k = 2 > K$; thus, it cannot be included. We can check similarly why cells incident with 29, 30, 40 for which $W = 1$, do not satisfy the conditions of Theorem II. But cell D incident with 55 having free weight $W = 1$, can be included.

Let us take W. The reduced weights of free vertices are shown in the fourth row of the weighting table.

Now, vertex 60 of $W = 0$, cannot still be included. With vertices 10, 21, 29, 30, 40, of weight $W = 1$, there is no cell incident satisfying conditions of Theorem II. With vertex 55 of weight $W = 1$ is incident cell D which takes 55's only neighbour 54 and for this all $k < K$; so row D is selected. The vertices 54, 55 are bound thereby. The weights of free vertices are computed and written in the fifth row of the weighting table. Another cell Y incident with 55 cannot be included. In the same way row J incident with 50 is selected and the free weights of the free vertices are reduced and entered in the sixth row of the weighting table. Next, row M incident with 32 is selected. The resulting reduced weights of the free vertices are shown in the seventh row of the weighting table. Now, two cells L and Q incident with 10, satisfy sufficient conditions for inclusion. We take L and reduce the weights of the free vertices. Note that when vertex 40 was unbound, L could not be included as an acceptable cell incident with 10). Next, incident with vertex 30 of $W = 0$, three cells, names, G, I, K satisfy sufficient conditions of inclusion. Let us take G, since it also bounds the free vertex 60 of free weight $W = 0$. The cells selected at the second step are indicated by two asterisks.

The form of the chart at this stage is shown in Fig. 3. Two vertices, 21 and 29 are still free, and Theorem II is not applicable to them.

THIRD STEP

When both theorems I and II cannot be applied any further, the general procedure will be to start with a vertex having smallest free weight and pick out the minimal form by trying all possible cells covering the neighbours of the vertex, and completing the minimal form for each trial, by a repetition of the second methodic step. In case, the second step made after a trial does not include all

the free vertices, a second trial is to be made, repeating a third step followed by another repetition of a second step. From all the trials, we call the one minimal which introduces minimum number of operations.

In the example that we have chosen, this step is trivial. The vertices 21 and 29 are selected by cell 'a' marked by three asteriks and there is no other alternative.

Thus one of the minimal forms of the Boolean Function given by Eq. (i) is

$$
\begin{aligned}
f = A+C+F+O+R+b & \qquad \text{(first step)} \\
+X+W+D+J+M+L+G & \qquad \text{(second step)} \\
+a & \qquad \text{(third step)} \qquad \ldots \quad \text{(iii)}
\end{aligned}
$$

To write the algebraic equivalent of a basic cell, for example, of the cell F given by 42, 46, 58, 62(4, 16) we write the leading number 42 in binary form, eliminate variable x_k whenever a difference 2^k appears in the bracket, and for the remaining digits '1' stands for an unprimed variable and '0' for a primed variable.

2^k	k	x_5	x_4	x_3	x_2	x_1	x_0		F
4, 16	2, 4	1	ϕ	1	ϕ	1	0	$= 42$	$x_5x_3x_1x'_0$

and so on for the other cells.

We can also obtain alternative minimal forms by interchanging cells without increasing the number of operations. Thus, we have seen that interchange is possible between W and U or L and Q, which will produce three more minimal forms. We also note that if L, M and D are not eliminated, we could interchange J with E producing a fourth minimal form and so on.

MODIFIED THIRD STEP AND CYCLIC BASIC CELL CHART

The third step of trial-repetition in both Svoboda's and McClusky's method is not very smooth. In fact when the cyclic basic cell chart (*) is considerably complex, there is no way out to break through the structure in McClusky's method. In Svoboda's method, however, there is one clue: start with vertices of smallest weights. At this point a modification might be introduced which will reduce the number of trial repetitions to a great extent. The modification is as follows:

(a) Start always with a vertex having smallest weight.

(b) Select the cell incident with the vertex which includes all the neighbours of the vertex. In case there are more than one such cells, selection of any one of them will suffice. But, if cells are incident with the chosen vertex which include not only the neighbours but other non-neighbour free vertices, select that row which includes the maximum number of non-neighbour free vertices. If this

*A basic cell chart is here said to be cyclic when with none of the vertices is incident a cell satisfying the conditions of both Theorem I and II.

number be the same for more than one cell, selection of any one of them will suffice.

(c) If a cell incident with a chosen vertex does not include all neighbours, select that cell which covers the maximum number of neighbours, and if there are more than one such cell, selection of any one of them will suffice. But, if there are cells incident with the vertex which not only includes the same maximum number of neighbours, but also some other non-neighbour free vertices, select that cell which includes the maximum number of non-neighbour free vertices. If this latter number be the same for more than one cell, selection of any one of the mwill suffice.

After each selection of a cell in (b) or (c) , reduce the weights of the free vertices and repeat the procedure until all the vertices are bound.

To illustrate the above procedure we choose a problem which can not be readily solved by McClusky's trial repetition method. McClusky gave an approximate solution of this problem by his method of selecting consistent-row set (McClusky, 1956).

The problem is to obtain the minimum sum of

$$f(x_3, x_2, x_1, x_0) = (0,\ 1,\ 2,\ 4,\ 5,\ 6,\ 7,\ 8,\ 9,\ 11,\ 13,\ 14,\ 15,\ 16,\ 18,\ 19,\ 20,\ 21,\ 23,\ 24,\ 25,\ 26,\ 27,\ 28,\ 29,\ 30) \qquad \ldots \text{(iv)}$$

The basic-cell chart, the weighting chart, and the weight reduction table are shown in Fig. 4. This is a cyclic basic cell chart. Incident with the vertex 30 of weight $W = 3$, there are two cells A and Z; neither of them covers all the neighbours of 30 viz., 14, 26, 28 so that criterion (b) is not applicable. Since A takes two neighbours and also a non-neighbour vertex 24, while Z only one. We select A [criterion (c)]. Columns heading 24, 26, 28, 30 are lined out, lining out extended to the weighting charts, reduced weights of free vertices are written in the second row of the weighting table (See Fig. 4). Now, the vertices 8 and 14 have free weight $W = 2$ and to both of them criterion (b) is applicable. The cell I incident with 14 takes two neighbours of 14 viz., 6, 15 and one non-neighbour free vertex 7. Also, cell W incident with vertex 8 takes the two neighbours of 8-0, 9 and one non-neighbour free vertex 1. Hence any one of the cells will do. Let us take I. The bound columns are lined out. Weights of the free vertices are reduced and entered in the third row of the weighting table. Now, vertices 2, 8, 11 have free weights $W = 2$. We can take either U or W or G at this stage, since all of them cover the free neighbours of 2, 8, 11 respectively and each has one non-neighbour free vertex, viz., 16, 1, 27 respectively. It is to be noted that vertex 23 also has free weight $W = 2$, but there is no cell incident covering all the free neighbours. Hence it is not considered. Let us take G and reduce the free weights.

The form of the charts after selection of A, I and G is shown in Fig. 5. Now, the vertex 8 has minimum free weight $W = 1$. We can select either W or S

[criterion (b)]. Let us take W and reduce weights of free vertices. Selection of U is now unique [criterion (b)]. Weights of free vertices are reduced and shown

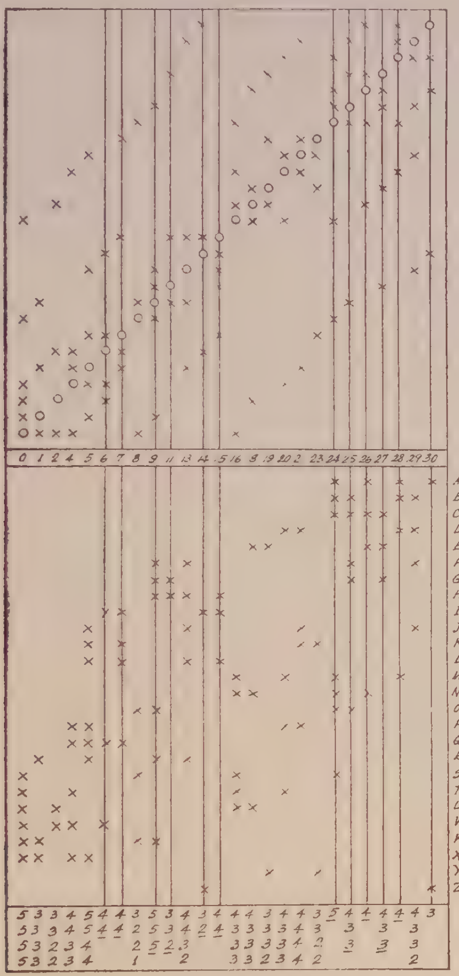

Fig. 5. The form of the charts after selection of cells A, I, G.

in the sixth row of the weighting table. Selection of Y is then unique. Free weights are reduced and shown in the seventh row. Then vertices 4, 13, 20, 29 have weights $W = 2$. Both 13 and 29 are covered by J and this cell besides providing for the neighbours, also include one non-neighbour free vertex. The cell P incident with 20, also satisfies similar conditions; let us, however, take J. This reduces free weights of 4 and 20 to $W = 1$. The condition of the charts is now shown in Fig. 6. We can include the vertices 4 and 20 at a time either by T or P. Let us take T. The minimal form, therefore, is

$$f = A+I+G+W+U+Y+J+T \qquad \dots \text{(v)}$$

Other minimal forms might also be obtained by interchanging cells so that the number of operations is not increased and each column contains at least one cross from a selected row. In our procedure described above, we have seen circumstances where alternative rows can be selected to obtain different minimal forms.

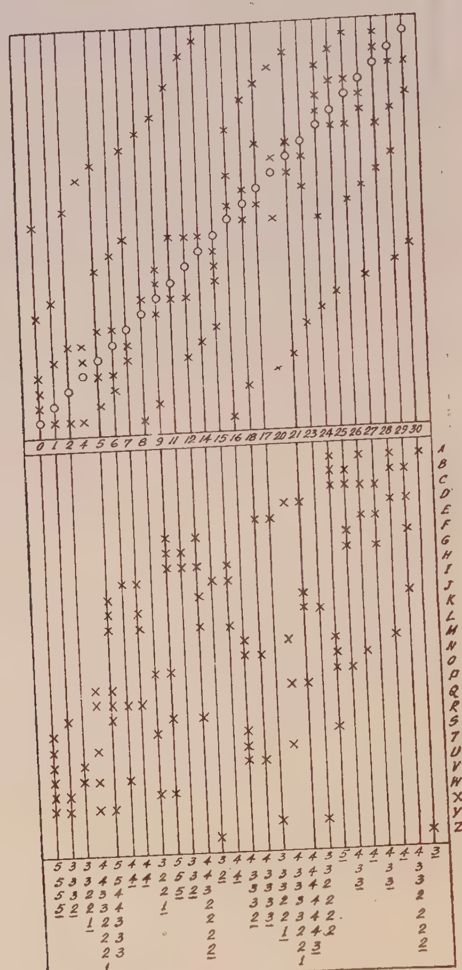

Fig. 6. The form of the charts after selection of cells A, I, G, W, U, Y and J.

The criterion (b) of the modified third step might sometimes give rise ambiguity, if there are many vertices having the same smallest weight. Th in the above problem initially there are eight vertices having weight $W =$ The question is : if we start with any of these vertices, is there any surety to a minimal form? The answer is 'in situations like this a minimal form is obtair only if we start with a vertex with which cells of different orders are incider

For example, with vertex 30 is incident a 2-cell A and a lower order cell—the 1-cell Z. Starting with 30, we have obtained the minimal form given by Eq. (v). Similar arguments apply to vertices 14, 19, 23 which have weight $W = 3$. Thus, starting with vertex 23, if we select cell K first, we obtain the minimum sum as

$$f = K+W+E+H+V+Z+B+M \qquad \dots \quad \text{(vi)}$$

which involve same number of operations as in (v). On the other hand, each of the vertices 1, 2, 8 and 11 has weight $W = 3$ and cells of order $K = 2$ are only incident; starting with any of them would not lead to a minimal solution. This guiding principle might also be applied at any stage of criterion (b) or (c) whenever we are faced with alternative choice.

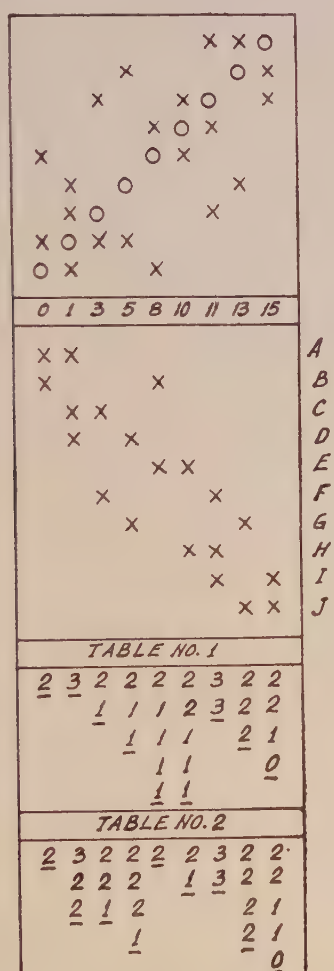

Fig. 7. The two alternative solutions for the functions expressed by Eq. (vii).

There are situations when all the alternative minimal forms can be obtained directly from one minimal form by interchange of variables or by priming variables or by both. For example, let us take the four variable function

$$f(x_3, x_2, x_1, x_0) = (0, 1, 3, 5, 8, 10, 11, 13, 15) \qquad \ldots \quad \text{(vii)}$$

The basic-cell chart, weighting chart and weight reduction table (for two trials) are shown in Fig. 7. If we start with vertex 0 and select cell A applying criterion (c) we shall obtain the minimum sum as

$$f_1 = A+F+G+E+\frac{J}{I} \qquad \ldots \quad \text{(viii)}$$

The sequence of operation is evident from weighting Table I. If, instead of A, we start with cell B, we shall obtain the solution (weighting Table II)

$$f_2 = B+H+C+G+\frac{J}{I} \qquad \ldots \quad \text{(ix)}$$

Now, f_2 can be directly obtained from f_1 by priming x_1 and x_3 and interchanging, since the above operation will leave the function unchanged; vertices 0, 1 are changed with vertices 10, 11 respectively so that cells A, E, F are changed to H, B, C respectively. This property of the function is called group invariance.

CONCLUSION

A method of minimisation of Boolean Functions in the form of a minimum sum has been presented in this paper by applying the methodical steps of Svoboda on McClusky's chart with the help of a weighting chart and a weight reduction table. The merit of this method is that it can be conveniently extended to cover cases involving more than six variables whereas the application of Svoboda's method to such cases becomes considerably inconvenient. Furthermore, in this method the basic cells incident with any vertex are easily obtained by looking along the column representing the vertex, whereas in Svoboda's method they will have to be searched out by several trials involving tossing and turning of the grids having different combinations.

A modification has been suggested on the third step of trial-repetition, which is particularly useful for minimising functions which form into cyclic basic cell charts.

The introduction of weighting chart has greatly systemetised the advantages of the methods of both Svoboda and McClusky.

ACKNOWLEDGMENT

The author wishes to express his indebtedness to Professor J. N. Bhar, D.Sc., F.N.I., for his keen interest in the work, and to Dr. A. K. Choudhury, M.Sc., D.Phil., for guidance and helpful discussions.

REFERENCES

Caldwell, S. H., 1958, Switching Circuits and Logical Design, John Wiley, New York.

Choudhury, A. K., 1959, *Journal of Inst. of Telecom. Engineers*, **5**, *June.*

Karnaugh, M., 1953, *Trans. A.I.E.E.*, **72**, Part I, Nov.

Keister, W., Ritchie, A. E., Washburn, S., 1951, The Design of Switching Circuits. D. Van Nostrand Co. Inc., New York.

McClusky, E. J. (Jr.), 1956, *Bell System Tech. Jour.*, **35**, 1417-1444.

Phister, Montgomery, Mr., 1958, Logical Design of Digital Computers. John Wiley & Sons, Inc.,

Shannon, C. E., 1938, *Trans. A.I.E.E.*, **57**, 713-723.

Svoboda, A., "Some Applications of Contact Grids" (Private Communication).

Svoboda, A., 1956, N.T.F–4, Nachrichtentechnische Fachberichte, Beihefte der NTZ, Publ. Fr. Vieweg & Sohn, Braunschweig "Graphical-mechanical aids for the synthesis of relay circuits".

Staff of Harvard Computation Laboratory, 1051, Synthesis of Electronic Computing and Control Circuits. Harvard University Press.

Troye, N. C. de., 1959, *Philips Research Reports*, **14**,

Urbano, R. H. and Mueller, R. K., 1956, *I.R.E. Trans. on Electronic Computers* *EC*–5, Sept.

NOTICE

No claims will be allowed for copies of journal lost in the mail or otherwise unless such claims are received within 4 months of the date of issue.

CONTENTS

Indian Journal of Physics Vol. 35, No. 1 January, 1961

		PAGE
1.	Effects of Coulomb Friction on the Performance of a Servomechanism having Backlash. Part II—Transient Response Considerations—A. K. Mahalanobis	1
2.	Raman Spectra of Para Fluorotoluene and Phenyl Acetonitrile in the Solid State at −180°C— Krishna Kumar Deb	16
3.	Dynamics of the Longitudinal Propagation of Elastic Disturbance Through a Medium Exhibiting Gradient of Elasticity— S. K. Ghosh	22
4.	Dispersion of Microwaves in Oxygen— Prem Swarup and S. K. Garg ...	28
5.	A Minimisation Method of Boolean Functions— Amarendra Mukhopadhyay	34

PRINTED BY KALIPADA MUKHERJEE, EKA PRESS, 204/1, B. T. ROAD, CALCUTTA-35
PUBLISHED BY THE REGISTRAR, INDIAN ASSOCIATION FOR THE CULTIVATION OF SCIENCE
2 & 3, LADY WILLINGDON ROAD, CALCUTTA-32